RSC Advances

PAPER

View Article Online
View Journal | View Issue

Cite this: *RSC Adv.*, 2023, **13**, 14594

Greener design and characterization of biochar/Fe_3O_4@SiO_2–Ag magnetic nanocomposite as efficient catalyst for synthesis of bioactive benzylpyrazolyl coumarin derivatives†

Dharmendra Dharmendra, Priyanka Chundawat, Yogeshwari Vyas, Purnima Chaubisa and Chetna Ameta *

Received 9th February 2023
Accepted 1st May 2023

DOI: 10.1039/d3ra00869j

rsc.li/rsc-advances

The study aimed to develop an efficient catalyst, biochar/Fe_3O_4@SiO_2–Ag magnetic nanocomposite, to synthesize bioactive benzylpyrazolyl coumarin derivatives through a one-pot multicomponent reaction. The catalyst was prepared using Ag nanoparticles synthesized with Lawsonia inermis leaf extract and carbon-based biochar obtained through pyrolysis of *Eucalyptus globulus* bark. The nanocomposite contained a silica-based interlayer, highly dispersed Ag nanoparticles, and a central magnetite core, which responded well to external fields. The biochar/Fe_3O_4@SiO_2–Ag nanocomposite showed excellent catalytic activity and could be easily recovered using an external magnet and reused five times without significant loss of performance. The resulting products were tested for antimicrobial activity and showed significant activity against various microorganisms.

Introduction

Human activities have led to unintentional contamination of the environment, prompting scientists to develop strategies for reducing pollution and designing processes that are both economically and environmentally friendly. Organic chemists have a crucial role in developing such strategies by systematically researching and designing processes that minimize environmental impacts. Green Chemistry is a promising approach that utilizes synthetic techniques and avoids the use of hazardous materials. It also involves the development of more efficient methods for producing heterocyclic chemicals that have potential applications in various fields.

The pharmaceutical industry and academic institutions are interested in developing straightforward and environmentally friendly reaction processes for synthesizing highly functionalized compound libraries of pharmaceutical motifs. Multicomponent reactions (MCRs) in green solvents have emerged as effective tools for developing such libraries and meeting the requirements of green chemistry due to their low cost, easy availability, and pertinent nature. The use of green solvents and efficient heterogeneous catalysts can significantly enhance the synthetic utility of these protocols.

Therefore, the primary objective of this research is to upgrade and simplify conventional processes to minimize environmental impacts while maintaining high efficiency and reducing economic costs. In this regard, the use of green solvents and efficient heterogeneous catalysts is gaining increasing attention as they can substantially improve the synthetic utility of MCRs. Such approaches can have a significant impact on the development of efficient and environmentally friendly processes for producing heterocyclic chemicals and other important compounds. Green solvent and efficient heterogeneous catalysts can substantially improve the synthetic utility of this kind of protocol.[1–6]

Researchers have recently become interested in biochar (BC), a renewable carbonaceous material made by thermochemical pyrolysing naturally occurring bio-waste in the lack of oxygen, due to its distinctive and fascinating physicochemical properties *i.e.* low cost, carbon-rich, high stability, non-toxicity, high porosity, adjustable surface function, and large specific surface area. Additionally, it possesses a lot of surface functional groups (C=O, COOH, and OH), which are highly customizable and may be used as a substrate to produce a variety of functional carbon compounds. Based on the aforementioned features, biochar has very excellent performances in a variety of study areas, including soil enhancement, recycling of agricultural waste, adsorption, reducing climate change, and conserving water.[7–16]

To establish low-cost and sustainable procedures for organic syntheses, heterogeneous catalysts are important. In comparison to conventional organic or inorganic homogeneous catalysts, the key benefits of these catalysts are the ability to recycle and reuse

Department of Chemistry, Mohanlal Sukhadia University, Udaipur, Rajasthan, India. E-mail: chetna.ameta@yahoo.com

† Electronic supplementary information (ESI) available. See DOI: https://doi.org/10.1039/d3ra00869j

catalytic materials, high surface area, easy control, low toxicity, simple separation, thermal stability, production of the desired products, and prevention of by-product formation. As such, using sustainable and green chemistry principles, magnetic catalysts are preferable for the synthesis of organic compounds. Due to synergistic effects, heat induction through the reaction mixture, simple and effective separation in the presence of an external magnetic field, easy catalyst recycling, high surface area that results in a high catalyst loading capacity, great dispersion, and the stabilization of active catalytic centers or organic functional groups on magnetic materials such as Fe_3O_4, $CoFe_2O_4$, $CuFe_2O_4$, $NiFe_2O_4$, *etc.* have recently widely used as alternative catalyst supports. Fe_3O_4 nanoparticles (NPs) outperform other magnetic materials in terms of magnetization properties. The magnetic catalyst can be recovered and reused with the help of an external magnetic field, magnetic separation is considered as a green technique. This can prevent the need of filtration or centrifugation steps in the separation process. However, the hydrophobic naked nano-ferrites have a high surface area to volume ratio, strong magnetic dipole–dipole attraction, and always have issues like self-aggregation and a lack of functional groups. The aggregation of magnetic nanoparticles can be successfully avoided by using biochar as a carrier. Functionalization and surface modification with organic or inorganic supports are required to address these issues and boost their effectiveness for the specific application.[17–22]

For Fe_3O_4 NPs, silica is also employed as a protective covering shell and the silica shell can prevent the aggregation of Fe_3O_4 nanoparticles. Furthermore, the high concentration of Si–OH groups on the surface of silica allows for further modification, especially by silicon reagents bearing organic bridges and suitable functional groups for subsequent modifications. In fact, more complex organic compounds with two or more functional groups can replace or modify the organic functional groups. Incorporating magnetic components into AgNPs-based catalysts has the potential to enhance the separation and recovery of nanosized Ag. However, magnetic particles are more sensitive and unstable than silver, particularly in acidic environments. To address this, silica can be used as a protective shell to cover the Fe_3O_4 particles, forming a core–shell (Fe_3O_4@SiO_2) structure. Previous studies have successfully developed techniques to synthesize Ag coated Fe_3O_4@SiO_2 composite microspheres using the Ag-mirror reaction. Despite these advances, there is still a need for simple and effective methods to produce small, highly dispersed AgNPs with a narrow size distribution on the Fe_3O_4@SiO_2 substrate.[23–27]

In both medical and synthetic chemistry, heterocyclic compounds with pyrazolone or coumarin scaffolds play

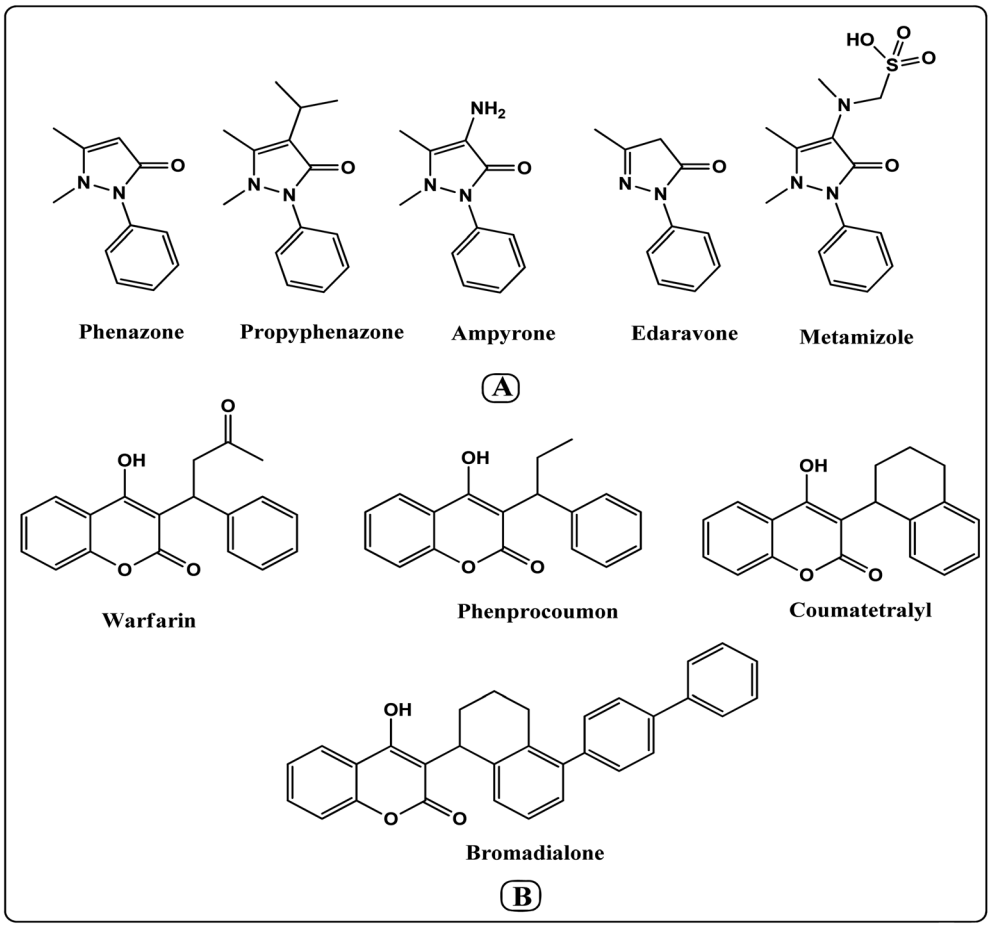

Fig. 1 Some of the commercial biologically active pyrazolone (A) and coumarin (B) derivatives.

significant roles because of their biological and pharmacological activities including antibacterial,[28] anti-viral,[29] anti-coagulant,[30] anti-HIV,[31] anti-oxidant, anti-inflammatory,[32] and antineoplastic activities.[33,34] Commercial examples include phenazone, propyphenazone, ampyrome, metamizole, edaravone, warfarin, phenprocoumon, coumatetralyl, and bromadialone, *etc.* (Fig. 1). Thus, the design of pyrazolone or coumarin derivatives has been done by chemists in the presence of various catalysts and green solvents. However, some of the described research may have drawbacks such as lengthy reaction periods, difficult catalyst separation, poor yields, and complicated purification techniques. Therefore, because of their various biological features, the simple design and synthesis of these derivatives are still necessary (Scheme 1).[35–38]

In this study, we aimed to develop an eco-friendly and effective heterogeneous catalyst for a one-pot four-component reaction to synthesize bioactive benzylpyrazolyl coumarin derivatives. The catalyst was designed, prepared, and characterized as a biochar/Fe_3O_4@SiO_2–Ag magnetic nano-composite. The reaction was carried out at 70 °C in a green solvent of EtOH : H_2O (1 : 1) with high efficiency and selectivity. The catalyst was synthesized using Lawsonia inermis leaf extract as a capping and reducing agent for Ag NPs, and biochar was obtained through pyrolysis of *Eucalyptus globulus* bark under low-oxygen conditions. The resulting nanocomposite was composed of a silica-based interlayer, highly dispersed Ag nanoparticles with a narrow size distribution, and a central magnetite core with a strong response to external fields. The catalyst could be recycled at least six times without a significant decrease in catalytic activity. The structures of the coumarin derivatives were characterized using FT-IR, ^{1}H NMR, and ^{13}C NMR spectroscopy. A plausible reaction mechanism was also proposed. Overall, this study provides a promising approach for the synthesis of biologically active compounds using an eco-friendly magnetic nano-composite catalyst.

When compared to the isolated solvents, the EtOH/H_2O combination exhibits noteworthy features that promote the Knoevenagel condensation when it has been established in the mixed solution:

(i) A stronger solvation strength as a result of the use of hydrogen bonds to bind molecular chains (cluster formation).

(ii) Stronger interactions with tiny polar molecules could be promoted by the mixtures' lower dielectric constants as compared to pure solvents.

(iii) The potential to increase organic molecule solubility as compared to using water as a solvent.

(iv) The ability to form cavities.[39–41]

Organic solvents, which are commonly used for various applications, are known to be hazardous to human health.[42] Examples of such solvents include toluene, DMF, acetone, and ethyl acetate. Therefore, safer alternatives such as ethanol/water (EtOH/H_2O) have been employed to reduce the risks associated with their use.

Experimental

Materials and methods

All of the chemicals were purchased from Sigma-Aldrich, Hi-Media, and Alfa-Aesar chemical companies. Open capillaries with Gallen Kamp's apparatus was used to measure the melting points of various substances and are uncorrected. Hitachi-PU 10 kV field emission-scanning electron microscope (FE-SEM), energy dispersive X-ray spectroscopy (EDX), and Hitachi (H-7500) 120 kV with CCD Camera HR-TEM (high resolution transmission electron microscope) were used to examine the surface morphology and size of the biochar/Fe_3O_4@SiO_2–Ag NPs nanocatalyst. The Perkin Elmer-Spectrum RX-IFTIR instrument was used to examine the FT-IR (Fourier transform infrared spectroscopy) spectra (ATR/KBr mode, cm^{-1}) of synthesized substances and nanocatalyst in the 400–4000 cm^{-1} range.

The JEOL JNM-ECZ400S was used to measure the ^{1}H and ^{13}C-NMR (nuclear magnetic resonance) spectra of synthesized compounds while operating at 100 to 400 MHz in DMSO-d_6 (dimethyl sulfoxide-d_6) as solvent and using TMS (tetramethylsilane) as an internal standard. Electrospray ionization mass spectra (ESI-MS) were recorded with waters micromass Q-TOF at SAIF, Chandigarh. The Panalytical's X'Pert Pro equipment (Powder XRD) was used to examine the crystal structure of biochar/Fe_3O_4@SiO_2–Ag magnetic nano-composite in the range of Bragg angle 2θ = 20° to 80°. A Lake Shore 7410 VSM (vibrating sample magnetometer) was used to assess the magnetic properties of nanoparticles. Additionally, the thermo-gravimetric analyzer (TGA; PerkinElmer STA 6000) was used to examine the thermal stability of prepared nanocatalyst while heating them at a rate of 10 °C min^{-1} in a N_2 atmosphere.

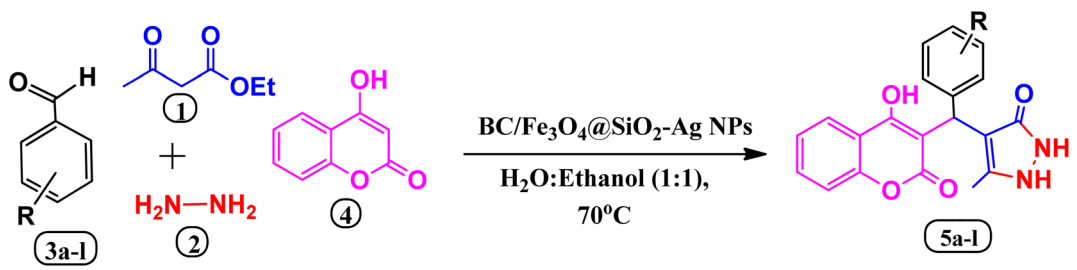

Scheme 1 An efficient MCR for the synthesis of benzylpyrazolylcoumarin in the presence of biochar/Fe_3O_4@SiO_2–Ag magnetic nano-composite.

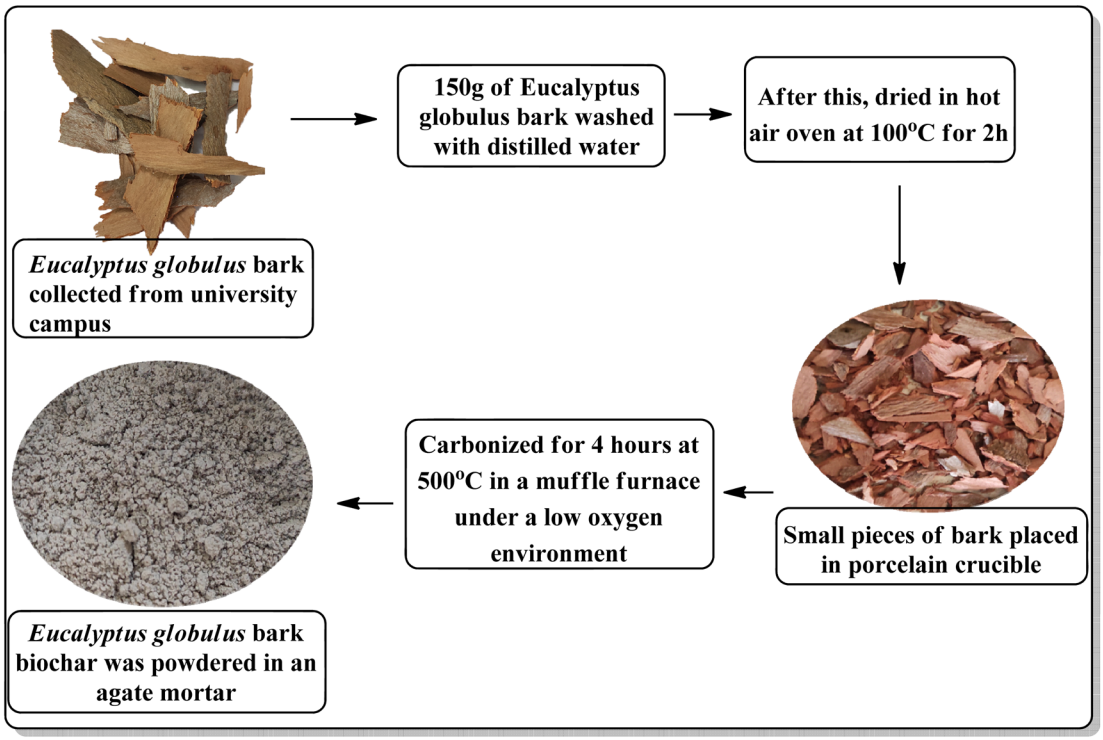

Fig. 2 Preparation of biochar from *Eucalyptus globulus* bark.

Design of biochar/Fe_3O_4@SiO_2–Ag magnetic nano-composite

Synthesis of biochar from *Eucalyptus globulus* bark. *Eucalyptus globulus* bark was collected from the campus of University College of Science, M. L. Sukhadia University, Udaipur (Rajasthan) INDIA. 150 g of *Eucalyptus globulus* bark washed with distilled water and dried in hot air oven at 100 °C for 2 h. Afterwards, an appropriate quantity of smaller pieces of *Eucalyptus globulus* bark were placed in a porcelain crucible and carbonized for 4 hours at 500 °C in a muffle furnace under a low oxygen environment (N_2 atmosphere inside the muffle furnace). Producing biochar under limited oxygen supply is crucial for several reasons. Firstly, it helps to reduce the amount of flue gas produced, particularly CO_2. Secondly, an oxygen-rich environment during the production of biochar can result in a lower quality material with high ash content and a reduced carbon surface area. Lastly, if carbon substrate reacts with O_2 molecules at high temperatures, it will lead to the production of CO_2, which reduces both the adsorbent properties and the number of active sites available on the biochar surface. Before being taken out of the furnace, the product was given time to cool naturally. The resulting *Eucalyptus globulus* bark biochar was powdered in an agate mortar and kept until needed in a plastic container (see Fig. 2).

Synthesis of biochar/Fe_3O_4 NPs. Modified chemical co-precipitation method was used to prepare the dried *Eucalyptus globulus* bark biochar with Fe_3O_4 to synthesis of biochar/Fe_3O_4 composite, also known as magnetic biochar (MB).[18,43,44] 5.0 g of prepared dried *Eucalyptus globulus* bark biochar and 3.0 g $FeSO_4 \cdot 7H_2O$ were mixed in 250 ml distilled water with constant stirring at 80 °C for 1 h. To obtain an iron hydroxide precipitate, freshly prepared hot NaOH solution was added drop-by-drop until the medium's pH was reached between 9 and 11. The resulting mixture was stirred for 1 hour and left at room temperature for 24 hours. Following filtration, the precipitate was extensively cleaned with distilled water and ethanol until it reached a pH of neutral, and then it was dried in an oven at 60 °C.

Synthesis of biochar/Fe_3O_4@SiO_2. The silica-coated magnetic Fe_3O_4 *Eucalyptus globulus* bark biochar (biochar/Fe_3O_4@SiO_2) was made by dissolving the suitable quantity of biochar/Fe_3O_4 in 100 ml ethanol, 20 ml distilled water, and 2.0 ml concentrated ammonia solution with constant stirring for 20 min. After that, 3 ml of tetraethyl orthosilicate (TEOS) was gradually added while the mixture was continuously stirred for 3 h at 35 °C. Using a permanent magnet to remove the silica-coated magnetic biochar from the solution, it was then rinsed with several times with deionized water and dried at 50 °C for 4 hours.[45]

Green synthesis of Ag nanoparticles from *Lawsonia inermis* leaves extract. In August 2022, healthy leaves of henna plant *Lawsonia inermis* (Fig. 1) were collected from Sojat city (Village bamboliya) in the Pali district of Rajasthan, North-west India. These *Lawsonia inermis* leaves were thoroughly cleansed with running tap water and then washed with distilled water. 15 g of fresh *Lawsonia inermis* leaves were added in 100 ml of double-distilled water at 60 °C for 1 h to obtain aqueous leaf extract. After cooling to ambient temperature, it was filtered through Whatman No. 1 filter paper to produce a transparent filtrate, which was then stored at 4 °C for use in future analyses.

Afterwards, 38 ml of a 1 mmol aqueous $AgNO_3$ solution were combined with 12 ml of this aqueous leaf extract with vigorously

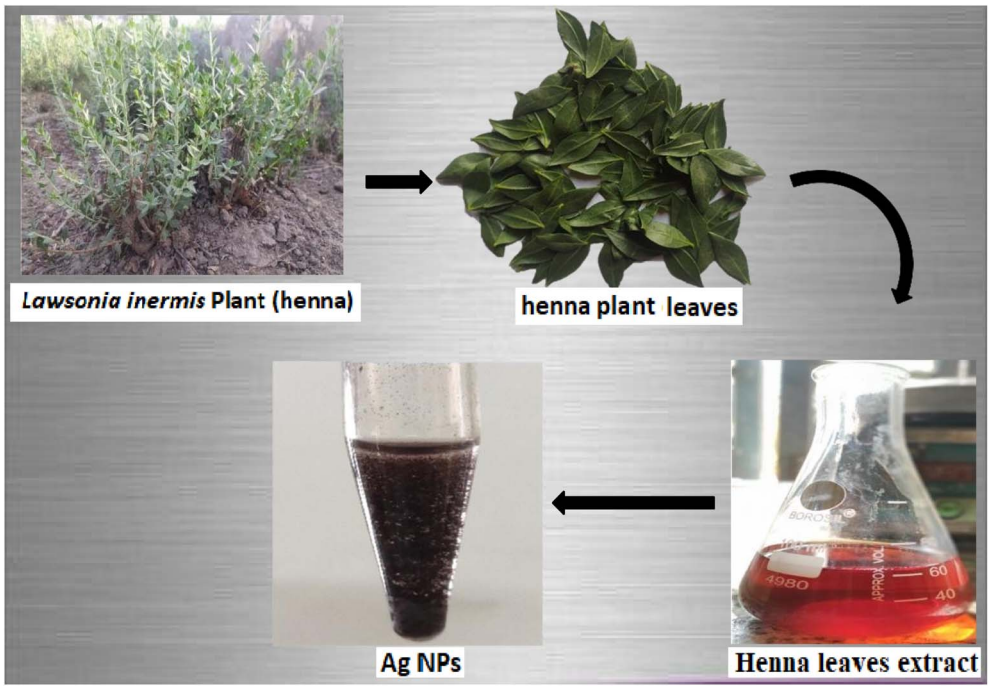

Fig. 3 Preparation of Ag NPs from *Lawsonia inermis* leaves extract.

stirring (700 rpm) for 3 h at 40–45 °C, a brownish-colored solution was produced. *Lawsonia inermis* leaves extract was used as a reducing and capping agent for the synthesis of AgNPs. Centrifugal ultrafiltration was used to concentrate, clean up Ag nanoparticles (Ag NPs) and then rinsed with deionized water (see Fig. 3).

Synthesis of biochar/Fe_3O_4@SiO_2–Ag MNPs. AgNPs were immobilised onto biochar/Fe_3O_4@SiO_2 using a simple *in situ* wet chemical procedure, resulting in a biochar/Fe_3O_4@SiO_2–Ag nanocomposite.[46] First, 0.5 g of biochar/Fe_3O_4@SiO_2 was dispersed into 100 ml of a 0.05 M ammonical silver nitrate solution with constant stirring at room temperature. Afterwards, for about 40 minutes, the $[Ag(NH_3)_2]^+$ ions were electrostatically attracted to the negatively charged Si–OH groups on the surfaces of the silica spheres. The dispersion was added to 20 ml of PVP (0.4 g) containing ethanol, and the mixture was heated for 4 hours at 70 °C. The desired products were magnetically separated, repeatedly rinsed in ethanol and deionized water, and then dried for 8 hours at 60 °C (see Fig. 4a and b).

General procedure for the synthesis of 4-((4-hydroxy-2-oxo-2*H*-chromen-3-yl)methyl)-5-methyl-1,2-dihydro-3*H*-pyrazo-3-one (5a–l). In a clean 50 ml round bottom flask with a reflux condenser, hydrazine hydrate (1 mmol), ethyl acetoacetate (1 mmol), and biochar/Fe_3O_4@SiO_2–Ag nanocomposite (0.4 g) as catalyst were added to 10 ml of EtOH : water (1 : 1) solution with constant stirring at 40 °C. Thenceforth, 4-hydroxycumarin (1 mmol), and aromatic aldehyde (1 mmol) were poured into the above mixture and refluxed for an appropriate time at 70 °C. TLC (thin layer chromatography) was used to monitor the progress of the reaction. The resultant reaction mass was filtered, cooled to room temperature, and then washed with distilled water followed by the re-crystallization of the obtained crude product with ethanol to produce a pure product. For reuse in subsequent runs, the catalyst was removed by an external magnet from the crude products during their crystallization.

Spectral data of selected products.[2,59–62]

*4-((4-Hydroxy-2-oxo-2H-chromen-3-yl)(phenyl)methyl)-5-methyl-1,2-dihydro-3H-pyrazol-3-one (**5a**).* White solid, m.p. 231–233 °C; FT-IR (ATR) (ν_{max}, cm^{-1}): 3015, 2881, 2824, 1704, 1607, 1363, 1182, 1028, 753; ^{1}H NMR (400 MHz, DMSO-d_6): δ 2.22 (3H, s), 2.46 (1H, d), 5.58 (1H, s), 7.10–7.20 (4H, m), 7.21–7.35 (4H, m),7.47–7.49 (1H, d, $J = 10.0$), 7.85–7.86 (1H, t, $J = 7.8$ Hz), 8.70 (1H, d, $J = 10.0$), 9.98(1H, s). ^{13}C NMR (100 MHz, DMSO-d_6): δ 10.61, 33.84, 40.16, 94.03, 105.17, 127.28, 128.54, 129.26, 131.92, 134.31, 152.72, 162.13, 165.21, 166.81, 168.14. MS (ESI) m/z for (348.35): 348.4449 $(M)^+$, 349.4409 $(M + 1)^+$.

*4-[(4-Hydroxy-2-oxo-2H-chromen-3-yl)-(2-hydroxy-phenyl)-methyl]-5-methyl-1,2-dihydro-pyrazol-3-one (**5b**).* White solid, m.p. 220–222 °C; FT-IR (ATR) (ν_{max}, cm^{-1}): 3181, 2964, 2723, 1664, 1607, 1448, 1363, 1190, 1043, 751; ^{1}H NMR (400 MHz, DMSO-d_6): δ 2.15 (3H, s),2.23 (1H, d), 5.05(1H, s), 5.64 (1H, s), 6.63–6.93 (4H, m), 7.22–7.36 (4H, m), 7.46–7.48 (1H, d, $J = 10.0$), 7.66–7.78 (1H, t, $J = 7.8$ Hz), 8.98 (1H, d, $J = 10.0$), 11.13 (1H, s). ^{13}C NMR (100 MHz, DMSO-d_6): δ 10.86, 18.90, 29.81, 40.88, 105.10, 107.27, 116.48, 119.54, 123.50, 127.81, 129.24, 131.01, 133.60, 153.00, 155.57, 159.13, 163.48, 164.77, 165.26, 166.16. MS (ESI) m/z for (364.35): 364.2721 $(M)^+$, 365.2701 $(M + 1)^+$.

*4-[(4-Hydroxy-2-oxo-2H-chromen-3-yl)-(4-hydroxy-phenyl)-methyl]-5-methyl-1,2-dihydro-pyrazol-3-one (**5c**).* White solid, m.p. 224–226 °C; FT-IR (ATR) (ν_{max}, cm^{-1}): 3029, 2880, 2710, 2310,1670, 1610, 1482, 1263, 1190, 884, 742; ^{1}H NMR (400 MHz, DMSO-d_6): δ 2.07 (3H, s), 2.14 (1H, d), 4.95 (1H, s), 5.22 (1H, s),

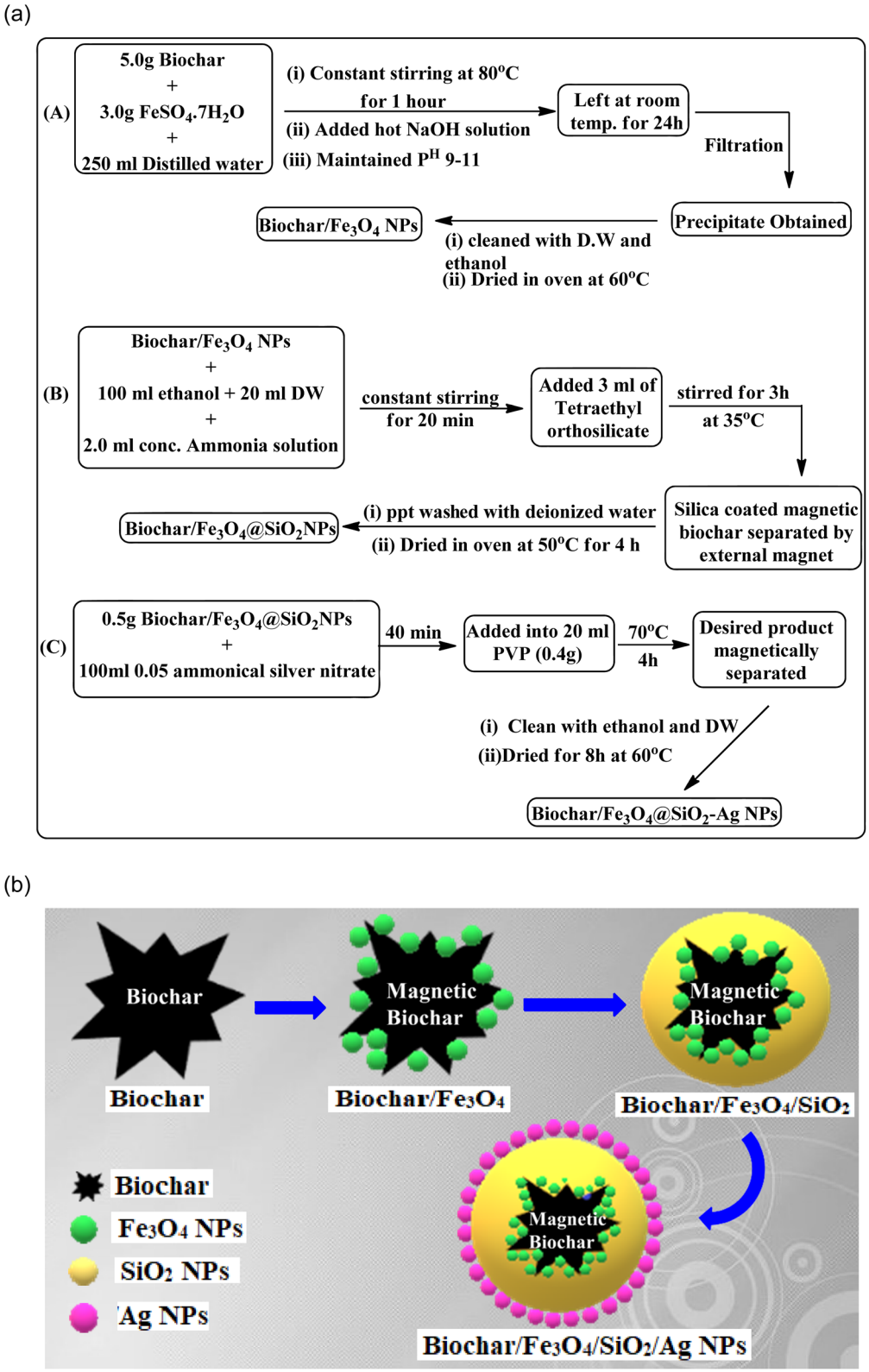

Fig. 4 (a) Synthesis of biochar/Fe_3O_4@SiO_2–Ag nanocomposite. (b) Synthesis of biochar/Fe_3O_4@SiO_2–Ag nanocomposite.

7.16–7.21 (3H, m), 7.47 (2H, m), 7.90 (2H, d), 8.34–8.36 (1H, t, J = 7.8 Hz), 8.91 (1H, d, J = 10.0), 11.69 (1H, s). ^{13}C NMR (100 MHz, DMSO-d_6): δ 10.98, 25.63, 30.89, 91.31, 105.67, 112.50, 121.11, 125.27, 126.76, 127.16, 128.42, 132.65, 150.72, 153.14, 155.70, 163.15, 166.83, 168.13. MS (ESI) m/z for (364.35): 364.2808 $(M)^+$, 365.5066 $(M + 1)^+$.

*4-[(4-Hydroxy-2-oxo-2H-chromen-3-yl)-(4-methoxy-phenyl)-methyl]-5-methyl-1,2-dihydro-pyrazol-3-one (**5d**).* White solid, m.p. 201–203 °C; FT-IR (ATR) (ν_{max}, cm^{-1}): 3514, 2991, 2881, 2383, 1685, 1598, 1500, 1448, 1159, 1243, 1018, 825; ^{1}H NMR (400 MHz, DMSO-d_6): δ 2.22 (3H, s), 2.46 (1H, d), 5.05(1H, s), 5.46 (3H, s), 6.28 (1H, s), 7.19–7.34 (4H, m), 7.49–7.51 (2H, m), 7.81 (1H, d, J = 10.0), 7.81 (1H, t, J = 7.8 Hz), 8.91 (1H, d, J = 10.0), 11.78 (1H, s). ^{13}C NMR (100 MHz, DMSO-d_6): δ 13.12, 23.64, 27.58, 58.50, 95.25, 106.00, 118.22, 118.72, 123.17, 126.10, 128.02, 129.22, 132.08, 152.73, 154.68, 161.17, 163.37, 166.28, 167.75. MS (ESI) m/z for (378.35): 377.3135 $(M)^+$, 379.3092 $(M + 1)^+$.

*4-[(4-Hydroxy-2-oxo-2H-chromen-3-yl)-(4-nitro-phenyl)-methyl]-5-methyl-1,2-dihydro-pyrazol-3-one (**5e**).* Light yellow solid, m.p. 209–211 °C; FT-IR (ATR) (ν_{max}, cm^{-1}): 2992, 2880, 2734, 2311, 1602, 1512, 1337, 1184, 1028, 754; ^{1}H NMR (400 MHz, DMSO-d_6): δ 2.09 (3H, s), 2.28 (1H, d), 5.60 (1H, s), 7.22–7.34 (4H, m), 7.73–7.75 (2H, m), 8.06–8.11 (2H, m), 8.83 (1H, d, J = 10.0), 10.66 (1H, s). ^{13}C NMR (100 MHz, DMSO-d_6): δ 10.25, 23.26, 27.25, 95.04, 105.47, 124.45, 124.97, 126.22, 128.47, 129.61, 131.44, 144.07, 146.12, 153.44, 155.22, 163.30, 165.55, 166.36, 167.15. MS (ESI) m/z for (393.35): 393.3372 $(M)^+$, 394.2322 $(M + 1)^+$.

*4-[(4-Hydroxy-2-oxo-2H-chromen-3-yl)-(3-nitro-phenyl)-methyl]-5-methyl-1,2-dihydro-pyrazol-3-one (**5f**).* Light yellow crystalline solid, m.p. 206–208 °C; FT-IR (ATR) (ν_{max}, cm^{-1}): 3064, 2880, 2756, 2310, 1610, 1521, 1345, 1188, 1098, 757; ^{1}H NMR (400 MHz, DMSO-d_6): δ 2.22 (3H, s), 2.32 (1H, d), 5.69 (1H, s), 7.19–7.25 (4H, m), 7.46–7.48 (4H, m), 7.57–7.59 (1H, d, J = 10.0), 7.78 (1H, d), 7.96 (1H, s), 8.96 (1H, d, J = 10.0), 10.80 (1H, s). ^{13}C NMR (100 MHz, DMSO-d_6): δ 10.59, 17.61, 33.84, 40.87, 92.72, 104.19, 116.28, 120.34, 121.86, 123.83, 124.65, 134.49, 144.19, 148.15, 152.10, 162.20, 164.77, 167.45, 168.73. MS (ESI) m/z for (393.35): 393.1624 $(M)^+$, 394.1246 $(M + 1)^+$.

*4-[(2-Chloro-phenyl)-(4-hydroxy-2-oxo-2H-chromen-3-yl)-methyl]-5-methyl-1,2-dihydro-pyrazol-3-one (**5i**).* White solid, m.p. 221–222 °C; FT-IR (ATR) (ν_{max}, cm^{-1}): 3367, 2882, 2825, 1605, 1432, 1269, 1201, 1038, 946, 743; ^{1}H NMR (400 MHz, DMSO-d_6): δ 2.03 (3H, s), 2.22 (1H, d), 5.57 (1H, s), 7.21–7.28 (4H, m), 7.45–7.57 (3H, m), 8.10 (1H, d, J = 10.0), 8.95 (1H, d, J = 10.0), 10.30 (1H, s). ^{13}C NMR (100 MHz, DMSO-d_6): δ 10.97, 25.28, 90.04, 105.63, 121.63, 125.56, 126.86, 127.46, 128.76, 130.76, 133.81, 135.23, 145.36, 147.25, 158.92, 161.25, 162.07. MS (ESI) m/z for (382.80): 382.2787 $(M)^+$, 384.1331 $(M + 2)^+$.

*4-[(4-Fluoro-phenyl)-(4-hydroxy-2-oxo-2H-chromen-3-yl)-methyl]-5-methyl-1,2-dihydro-pyrazol-3-one (**5j**).* White solid, m.p. 237–238 °C; FT-IR (ATR) (ν_{max}, cm^{-1}): 3004, 2880, 2697, 1895, 1590, 1495, 1401, 1288, 1216, 1142, 951, 821; ^{1}H NMR (400 MHz, DMSO-d_6): δ 2.06 (3H, s), 2.21 (1H, d), 5.49 (1H, s), 6.99–7.09 (4H, m), 7.30–7.34 (2H, m), 7.89–7.92 (2H, m), 8.96 (1H, d, J = 10.0), 9.95 (1H, s). ^{13}C NMR (100 MHz, DMSO-d_6): δ 10.01, 25.88, 30.87, 91.86, 105.58, 116.75, 126.22, 126.82, 131.20, 134.80, 151.81, 153.66, 161.09, 163.07, 165.51, 166.80. MS (ESI) m/z for (366.34): 366.1648 $(M)^+$, 368.1662 $(M + 2)^+$.

*4-[(3a,7a-Dihydro-1H-indol-3-yl)-(4-hydroxy-2-oxo-2H-chromen-3-yl)-methyl]-5-methyl-1,2-dihydro-pyrazol-3-one (**5k**).* Cream crystalline solid, m.p. 236–238 °C; FT-IR (ATR) (ν_{max}, cm^{-1}): 3179, 3048, 2880, 2825, 2306, 1673, 1505, 1432, 1282, 1120, 1011, 737; ^{1}H NMR (400 MHz, DMSO-d_6): δ 2.07 (3H, s), 2.14 (1H, d), 2.46 (1H, s), 4.96 (1H, d), 5.22 (1H, t), 5.56 (1H, s), 7.14–7.18 (4H, m), 7.19–7.23(4H, m), 7.45 (1H, d, J = 10.0), 7.90 (1H, t), 8.36(1H, d), 8.91 (1H, d, J = 10.0), 11.70 (1H, s). ^{13}C NMR (100 MHz, DMSO-d_6): δ 10.98, 21.97, 25.92, 41.76, 53.93, 95.79, 105.88, 113.07, 116.48, 121.31, 122.60, 123.5, 125.5, 127.06, 129.24, 132.31, 155.56, 161.70, 163.10, 167.70, 166.54. MS (ESI) m/z for (389.40): 389.3981 $(M)^+$, 390.1929 $(M + 1)^+$.

Result and discussion

Characterization of biochar/Fe_3O_4@SiO_2–Ag magnetic nanocomposite

FT-IR spectra analysis of Ag NPs and biochar/Fe_3O_4@SiO_2–Ag MNC. FT-IR spectra were measured to confirm the composition and structure of the nano-composite. The FT-IR of the catalyst at various stages is shown in Fig. 5: (a) biochar, (b) biochar/Fe_3O_4 particles, (c) biochar/Fe_3O_4@SiO_2 particles, and (d) biochar/Fe_3O_4@SiO_2–Ag MNC. The characteristic BC (biochar) bands for C=C stretching of the aromatic ring are shown in Fig. 5a at 1557 cm^{-1}. The O–H bending of the polyphenol is confirmed by the band at 1398 cm^{-1}, which also indicates the presence of an aromatic group. In addition, the absorption band at 1073 cm^{-1} was ascribed to the C–O–C and secondary O–H groups. The band near the 835 cm^{-1} can be attributed to C=C symmetric stretching and the peak of the O–H stretching can also be seen at 3140 cm^{-1}. These bands show that the biochar (BC) sample's surface has a high concentration of functional groups, which is beneficial for further modifying carbon-based nanomaterial.

Fe_3O_4 microspheres exhibit characteristic bands at 595 and 615 cm^{-1}, which are related to the Fe–O stretches, as seen in Fig. 5b. The new bands in the Fe_3O_4@SiO_2 microspheres are focused around 895 cm^{-1} and 1050–1090 cm^{-1} (Fig. 5c). The band at 1050–1090 cm^{-1} was assigned to the asymmetric stretching vibration of Si–O–Si, whereas the new absorption at 895 cm^{-1} can be attributed to the symmetric vibration of Si–O–Si. These findings show that SiO_2 is immobilized on the Fe_3O_4 microsphere surfaces. In Fig. 5d, the peak deviations of Ag NPs observed at 2985 cm^{-1} and 1632 cm^{-1}. It clearly suggests that the successfully formation of biochar/Fe_3O_4@SiO_2–Ag magnetic nanocatalyst (MNC).

In FT-IR spectra of synthesized Ag NPs (Fig. 6a), the strong peaks were visible at 3380 cm^{-1} represents the N–H stretch (primary, secondary amines, and amides) arising from the peptide linkages present in the proteins of the extract, 1631.41 cm^{-1} for C–C stretch (in-ring) aromatics, 1615 cm^{-1} for C–C stretch (in-ring) aromatics, 1370 cm^{-1} stands for C–C and C–N stretching, and 1054 cm^{-1} stands for C–N stretch (aliphatic amines), and an absorption peak exhibited at wavenumber 600–500 cm^{-1} which is associated to the stretching mode of Ag nanoparticles. So that, the proteins could most possibly form a coat covering on the metal nanoparticles (capping of silver nanoparticles) for prevent agglomeration of the particles and stabilizing them in the medium.[47] Recyclability of catalysts is

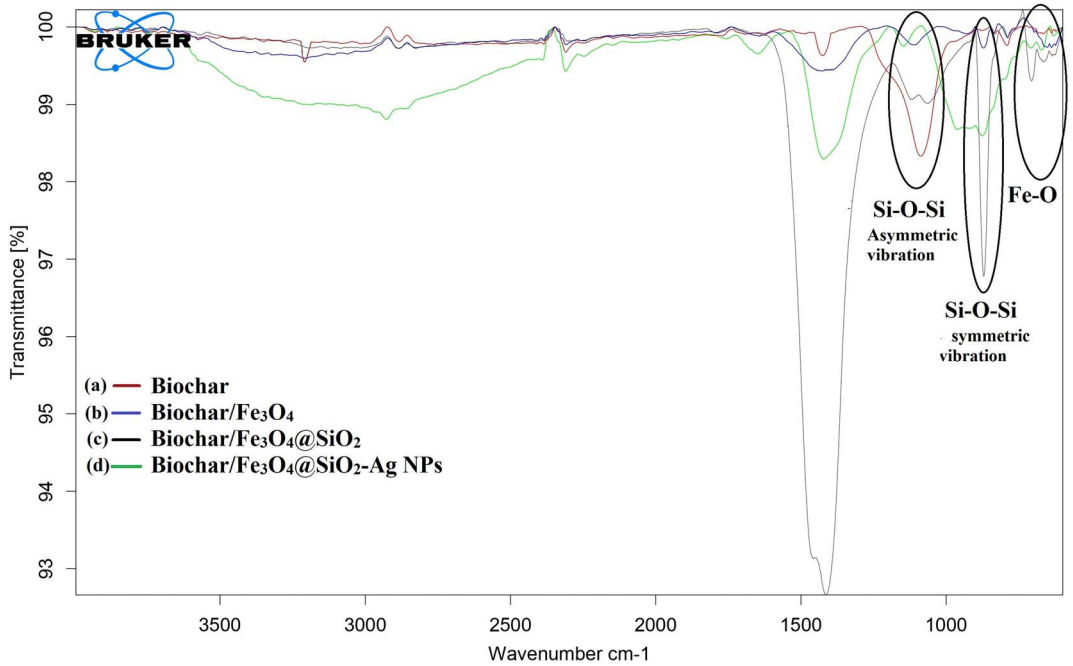

Fig. 5 FT-IR spectra of (a) biochar (red), (b) biochar/Fe_3O_4 (blue), (c) biochar/Fe_3O_4@SiO_2 (black), (d) biochar/Fe_3O_4@SiO_2–Ag MNC (green).

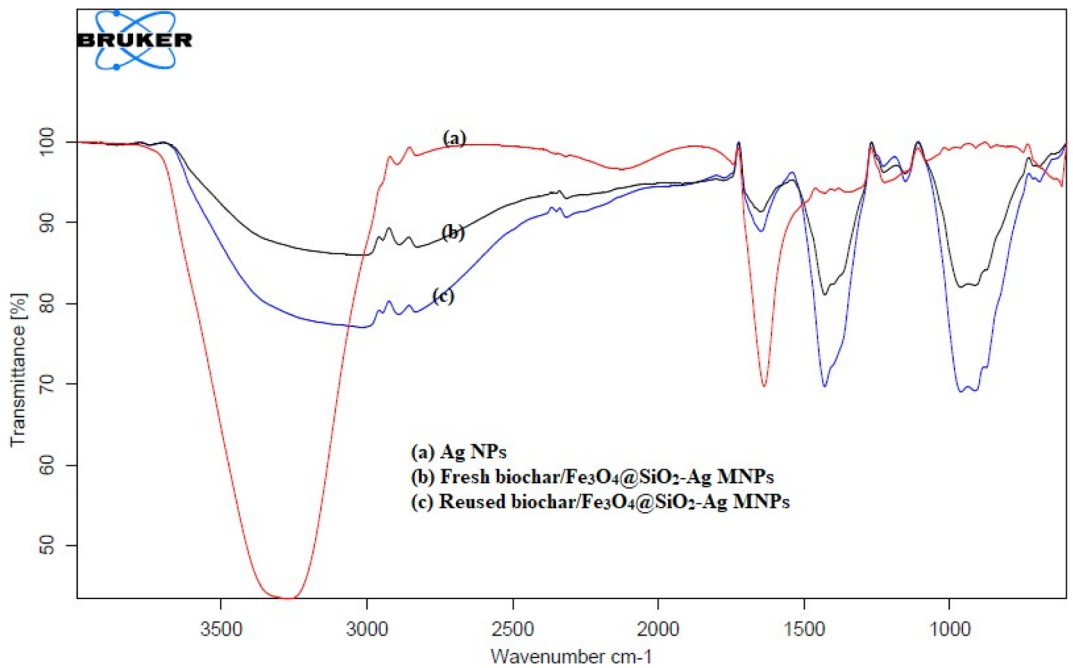

Fig. 6 FT-IR spectra of (a) Ag NPs (red), (b) fresh biochar/Fe_3O_4@SiO_2–Ag MNPs (black), and (c) reused biochar/Fe_3O_4@SiO_2–Ag MNPs (blue).

essential for more cost-effective operations. As a result, the recyclability of catalysts was examined over five reaction cycles. The FT-IR spectra of fresh (Fig. 6b) and reused (Fig. 6c) catalyst shown that the composite was still stable and exhibited a high catalytic activity.[45,46]

UV-visible spectra of Ag NPs. The formation of Ag NPs by the *L. inermis* aqueous leaf extract was observed using a UV-visible (UV-vis) spectrophotometer. After 24 hours of moderate stirring at room temperature, the reaction mixture's UV-vis absorbance was measured in order to confirm the reduction of silver ions. In the measurement, distilled water was used as a reference. Synthesized Ag NPs in an aliquot volume of 0.5 ml were diluted in 2 ml of Milli-Q water. A double-beam Shimadzu (UV-1780) UV-visible spectrophotometer was used to measure the Ag

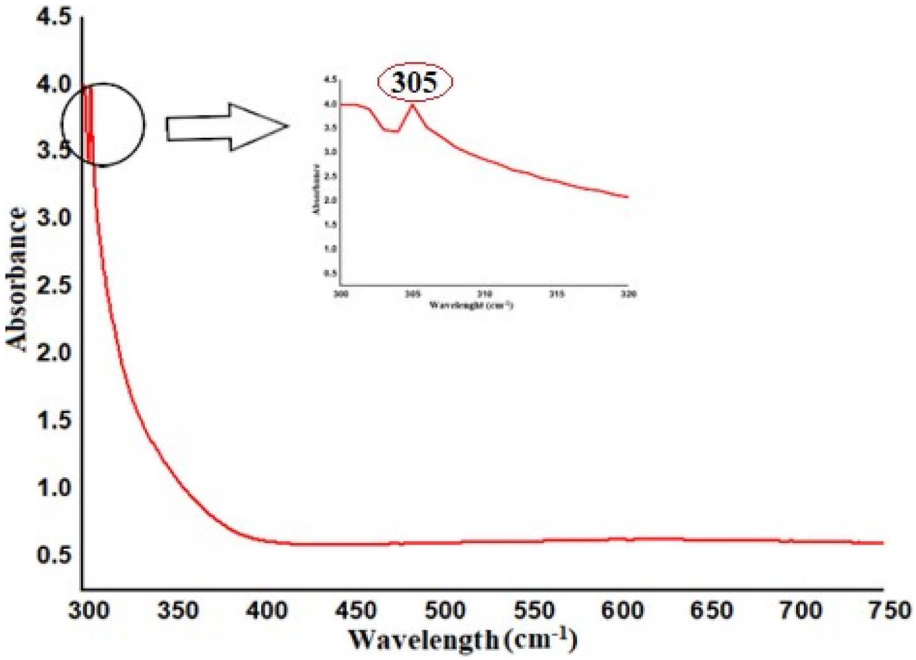

Fig. 7 UV-visible spectra of Ag NPs.

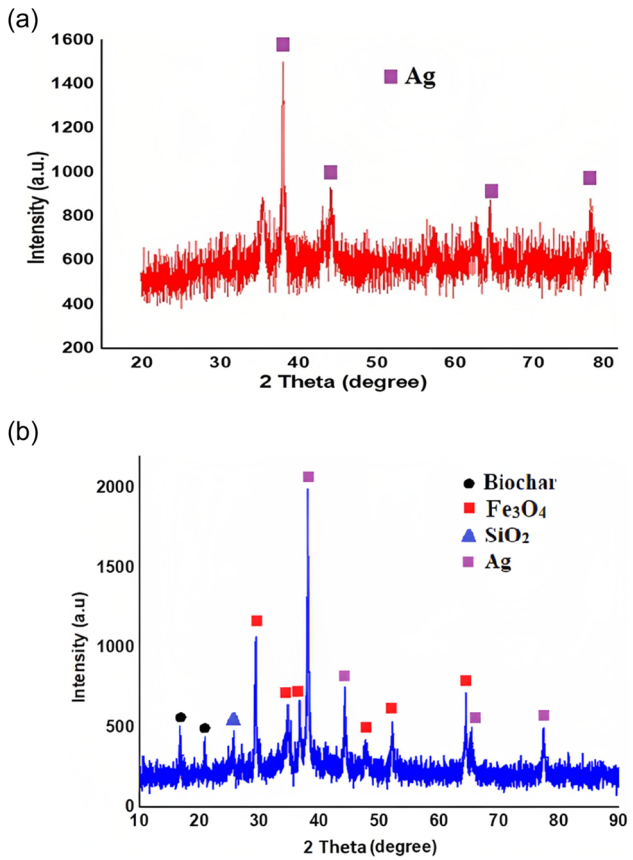

Fig. 8 (a) XRD patterns of the synthesized Ag NPs. (b) The XRD measurement of the biochar/Fe_3O_4@SiO_2–Ag MNPs.

NPs with continuous scanning from 300 to 750 nm with a significant peak at 305 nm (Fig. 7). Because this peak falls within the region of the surface plasmon resonance (SPR) for Ag NPs, it confirmed that Ag NPs have formed.[48,49]

XRD analysis of Ag and biochar/Fe_3O_4@SiO_2–Ag MNC. Fig. 8a displays the XRD patterns of the Ag NPs synthesized by *L. inermis* aqueous leaf extract. At the diffraction angles (2θ) = 38.16°, 44.38°, 64.52°, and 77.42°which correspond to the Miller indices (111), (200), (220), and (311) respectively, it exhibits four strong diffraction peaks. This demonstrates that the face centered cubic (FCC) structure with a preferential orientation in the 111 direction is present in the prepared Ag-NPs samples.[50] The XRD measurement of the biochar/Fe_3O_4@SiO_2–Ag MNPs (magnetic nanoparticles) is shown in Fig. 8b. This pattern showed a distinctive peak at $2\theta = 20.5°$ [crystal plane index C(002)], which is related to the parallel and azimuthal orientation of the aromatic and carbonised structure. A high degree of orientation is indicated by the sharp peak. Moreover, the absence of γ-bands connected to amorphous and aliphatic structures is shown by the high symmetry of the C(002) peak.[51,52] A broad peak of amorphous SiO_2 could be found between 2θ = 24.68° to 25.72°. The diffraction peaks of Fe_3O_4 at $2\theta = 64.42°$, 52.18°, 47.72°, 34.74°, and 29.38° were assigned to the reflection planes of the (440), (511), (400), (311), and (220).[53] Furthermore, the major peaks appeared at $2\theta = 38.08°$, 44.24°, 64.44°, and 77.17°, which could be assigned to (111), (200), (220), and (311) planes of Ag NPs, respectively (see Fig. 8b).

HR-TEM and FE-SEM study of nanocomposite. HR-TEM was used to examine the morphologies and structures of the catalyst. The HR-TEM picture of biochar/Fe_3O_4@SiO_2–Ag MNPs is shown in Fig. 9a–d, where well-dispersed spherical and rod shape particles with an average diameter of around 20–30 nm were

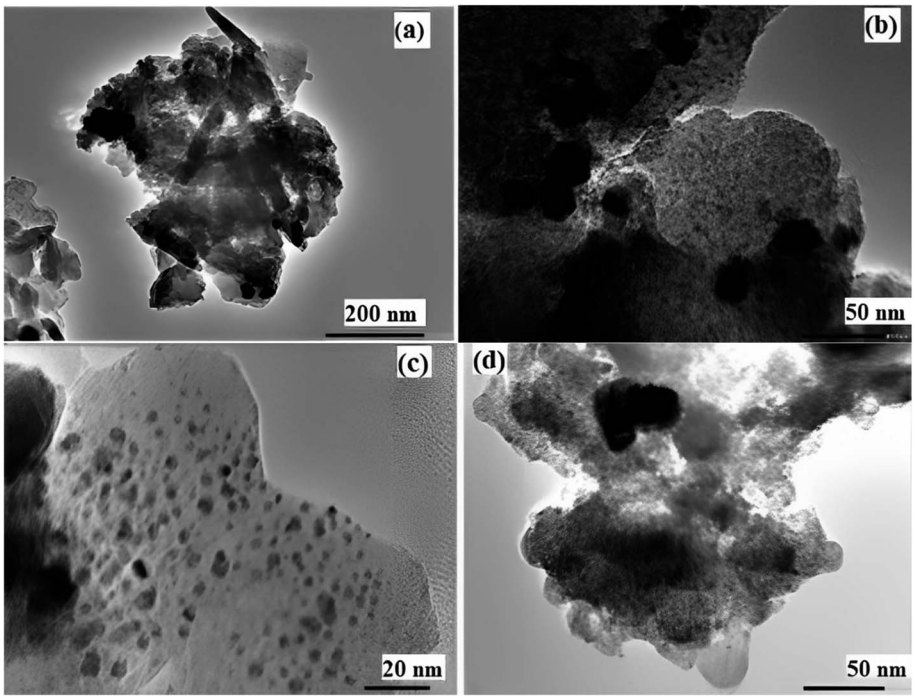

Fig. 9 (a)–(d) HR-TEM images of biochar/Fe_3O_4@SiO_2–Ag MNP.

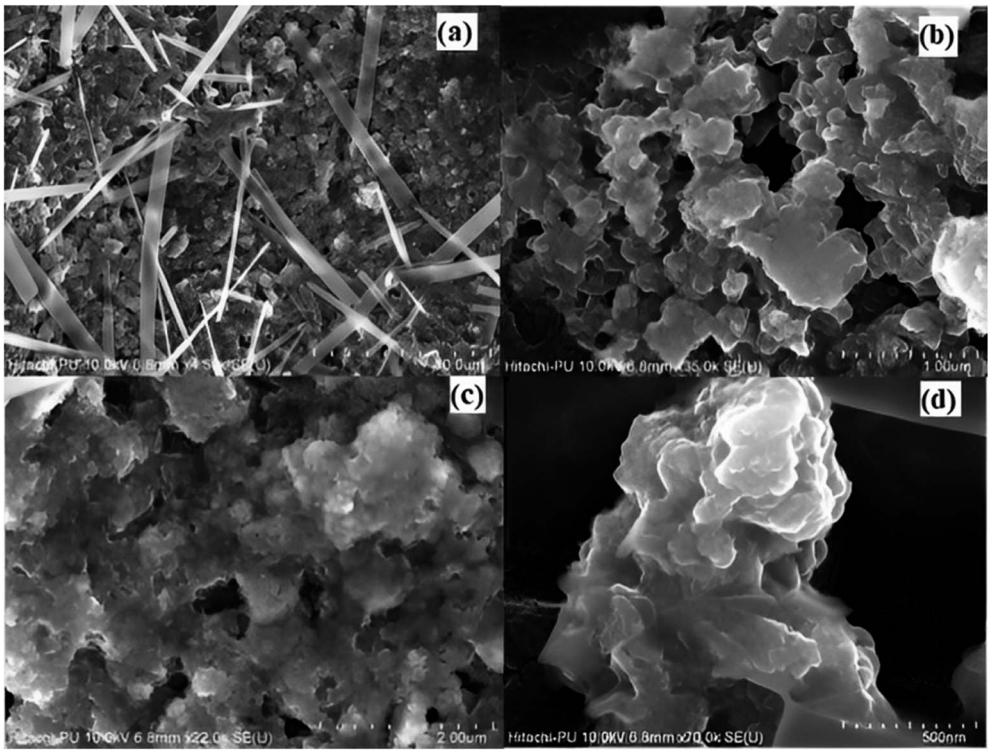

Fig. 10 (a)–(d) FE-SEM images of biochar/Fe_3O_4@SiO_2–Ag MNP.

clearly visible. In Fig. 8a–d, which exhibits the TEM image of the biochar/Fe_3O_4@SiO_2–Ag particles, small nanoparticles are evenly dispersed on the surface of the biochar/Fe_3O_4@SiO_2 particles.

The FE-SEM images of the catalyst are shown in Fig. 10a–d. The FE-SEM image depicts the porous honeycomb like structure with spherical and rod-like shape of biochar/Fe_3O_4@SiO_2–Ag MNPs. To further analyze the structure of the biochar/

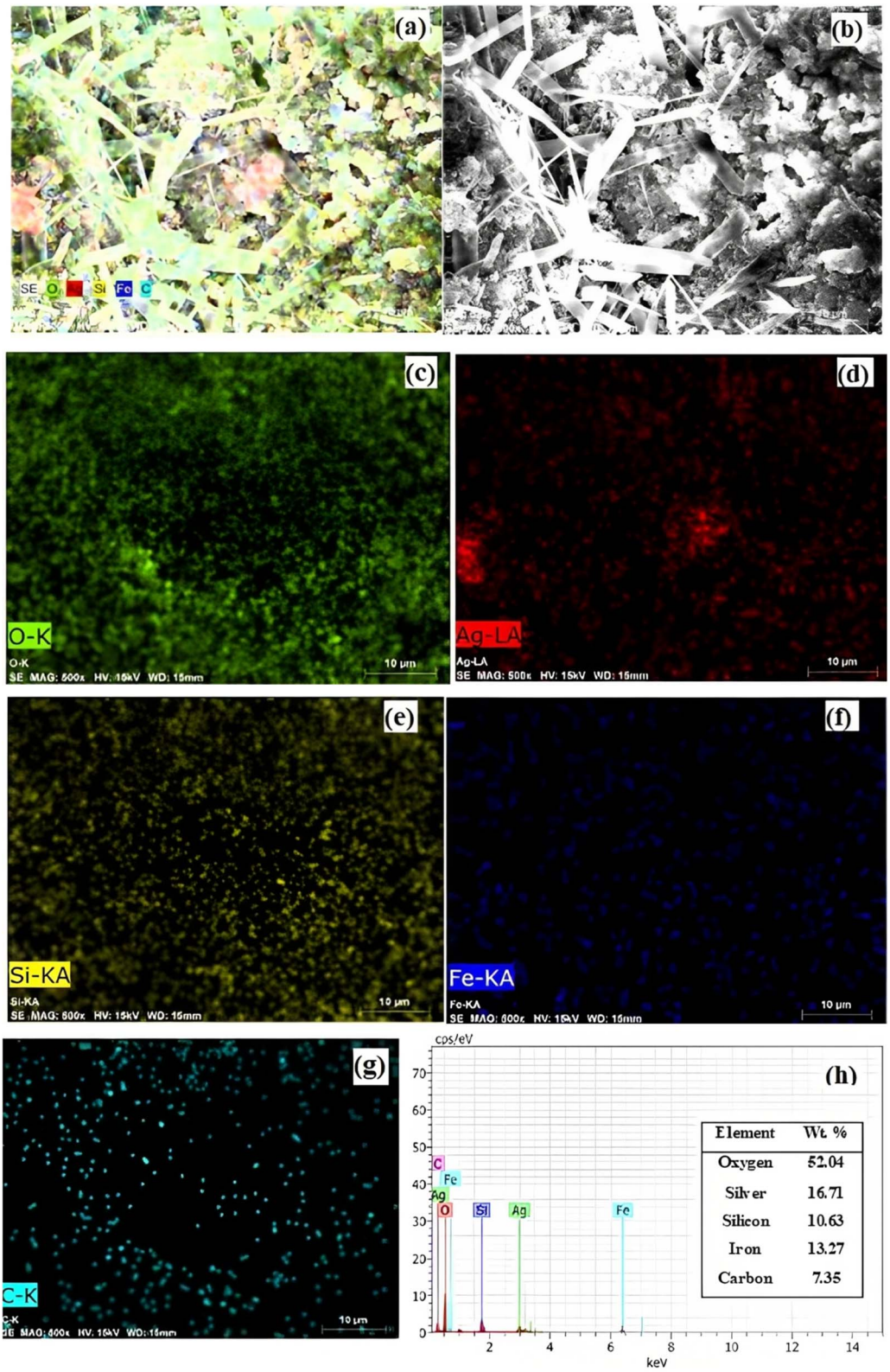

Fig. 11 (a)–(h) FE-SEM mapping and EDAX images of biochar/Fe_3O_4@SiO_2–Ag MNPs.

Fe_3O_4@SiO_2–Ag nanocomposite, the distribution of the components on its surface was revealed using the EDS mapping technique. Fig. 11a–h shows the EDS mapping images of this nanocomposite. The analysis confirmed the presence of C (7.35%), O (52.04%), Fe (13.27%), Si (10.63%), and Ag (16.71%) components in the structure of the biochar/Fe_3O_4–TiO_2

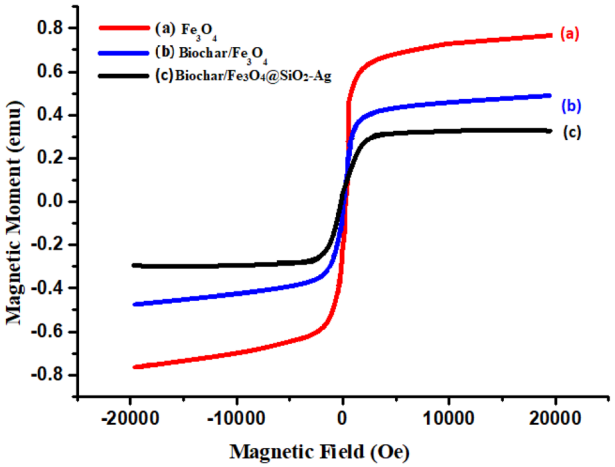

Fig. 12 Magnetization curves of (a) Fe_3O_4, (b) biochar/Fe_3O_4, and (c) biochar/Fe_3O_4@SiO_2–Ag nano-composite.

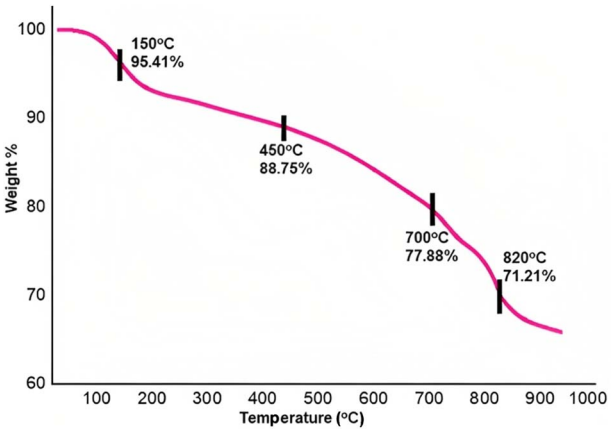

Fig. 13 TGA curves of biochar/Fe_3O_4@SiO_2–Ag nanocomposite.

nanocatalyst, showing that Fe_3O_4, SiO_2, and Ag nanoparticles were consolidated on the carbon-based biochar substrate.

VSM study of nanocomposite. As previously noted, the efficiency of a catalyst in aqueous solution greatly depends on the separation and recovery of nanoparticles. Small catalyst particle separation involves complex procedures that have low efficiency and raise the cost of practical. While using magnetic particles permits the nanoparticles to quickly separate from the solution when using an external magnetic field. Magnetic properties of the synthesized catalyst were evaluated using a Lake Shore 7410 VSM vibrating sample magnetometer at room temperature (Fig. 12). The results shown in Fig. 12–c indicated that there is no hysteresis loop in the magnetization curve, confirming that the synthesized biochar/Fe_3O_4@SiO_2–Ag nano-composite is superparamagnetic and can be easily isolated from the solution by an external magnetite field. The magnetization saturation (M_s) values of pure Fe_3O_4 (Fig. 12a), biochar/Fe_3O_4 (Fig. 12b), and the biochar/Fe_3O_4@SiO_2–Ag nanocomposite (Fig. 12c) are 0.15, 0.43, and 0.31 emu, respectively. The M_s value of Fe_3O_4 is higher than that of biochar/Fe_3O_4 microspheres and Fe_3O_4@SiO_2–Ag nanocomposite due to the SiO_2 shell's inclusion. The coating thickness was a contributing factor in this reduction of M_s value. The reduction in magnetic saturation properties increased with coating thickness. Biochar/Fe_3O_4@SiO_2–Ag nanocomposite has a slightly lower M_s value than biochar/Fe_3O_4, which is due to the slight increase in mass and size brought on by the deposition of SiO_2 and Ag NPs on the surfaces of biochar/Fe_3O_4. It should be observed that the biochar/Fe_3O_4@SiO_2–Ag nanocomposite exhibits significant magnetization, indicating its appropriateness for magnetic recovery and separation.[54–56]

TGA of nano-composite. Thermo gravimetric analysis (TGA) is a method of thermal analysis where variations in chemical and physical properties of materials are evaluated under the influence of a continuous rise in temperature or, as a function of time, having non-varying temperature and mass loss. To assess the thermal stability of the samples, the TGA analysis was performed under air atmosphere. The TGA results for biochar/Fe_3O_4@SiO_2–Ag nano-composite are displayed in Fig. 13. TGA analysis of biochar/Fe_3O_4@SiO_2–Ag nano-composite revealed a consistent weight decrease at temperatures above 120 °C. The first weight loss around 4.59% at temperature range between 120 °C to 150 °C was due to the removal of physically adsorbable water and solvent on the surface of biochar/Fe_3O_4@SiO_2–Ag nano-composite. Due to the dehydration of hydroxyl groups and decomposition of the remaining organic constituent, a second weight loss of approximate 10% was observed between 200 °C to 500 °C. The third weight loss above 500 °C (20.75%) is due to the thermal phase change of the material. According to the TGA curves, the catalyst in this investigation maintained higher residual mass (>65%) at 950 °C and proved to be more thermally stable.[57,58]

The study of catalytic activity of biochar/Fe_3O_4@SiO_2–Ag MNPs in the synthesis of benzylpyrazolyl coumarins derivatives. The modal reaction was investigated using a variety of catalysts, temperature and solvents, in an effort to recognise the optimization of the reaction conditions and to increase the product yield in a short period of time (Tables 1 and 2).

The synthesis involving benzaldehyde (1 mmol), ethyl acetoacetate (1 mmol), hydrazine (1 mmol), and 4-hydroxycoumarin (1 mmol) was chosen as the model process for synthesizing 4-((4-hydroxy-2-oxo-2*H*-chromen-3-yl)(phenyl) methyl)-5-methyl-2,4-dihydro-3*H*-pyrazol-3-one (**5a**). Different conditions, including various solvents, temperatures, and catalyst amounts, were used to explore this reaction. The modal Reaction was refluxed in the presence of water and ethanol as the solvent without the presence of a catalyst, however even after 120 min., no products were produced (Table 2, entry 1). Then the reaction was performed under solvent free condition at room temperature in the presence of catalyst for 150 min., no product yield obtained (Table 1, entry 1). After this, the model reaction was carried out in the presence of water and ethanol at room temperature to 60 °C, 55–75% yield produced respectively (Table 1, entry 3–5). Then the modal reaction was also performed under microwave, ultrasound irradiation, and at room temperature

Table 1 The modal condensation reaction of ethyl acetoacetate (1 mmol), hydrazine hydrate (1 mmol), 4-hydroxycoumarin (1 mmol), and benzaldehyde (1 mmol) under various conditions

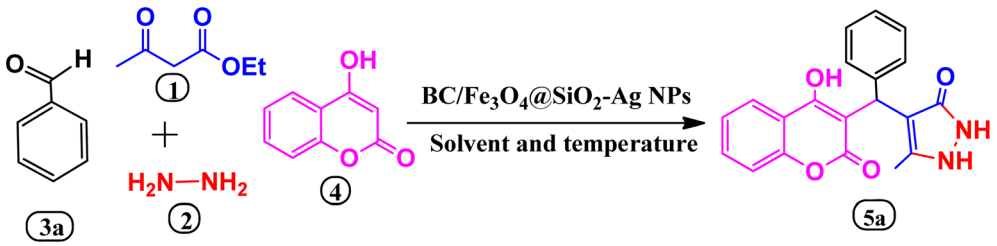

Entry	Solvent	Condition	Time (min)	Yield[a] %
1	Solvent free	R. T.	150	0
2	Solvent free	80 °C	95	30
3	H_2O	R. T.	60	55
4	H_2O	60 °C	35	75
5	EtOH	R. T.	60	60
5	EtOH	60 °C	30	75
6	H_2O/EtOH(1 : 1)	Microwave	8	84
7	H_2O/EtOH(1 : 1)	Ultrasonic	30	80
8	H_2O/EtOH(1 : 1)	R. T.	60	75
9	**H2O/EtOH(1 : 1)**	**70 °C**	**12**	**97**
10	H_2O/EtOH(1 : 2)	70 °C	15	90
11	H_2O/EtOH(2 : 1)	70 °C	15	88
12	H_2O/EtOH(1 : 1)	80 °C	12	97
13	H_2O/EtOH(1 : 1)	100 °C	12	97

[a] Isolated yield.

Table 2 The modal condensation reaction of ethyl acetoacetate (1 mmol), hydrazine hydrate (1 mmol), 4-hydroxycoumarin (1 mmol) and benzaldehyde (1 mmol) in the presence of various amounts of biochar/Fe_3O_4@SiO_2–Ag MNPs[a]

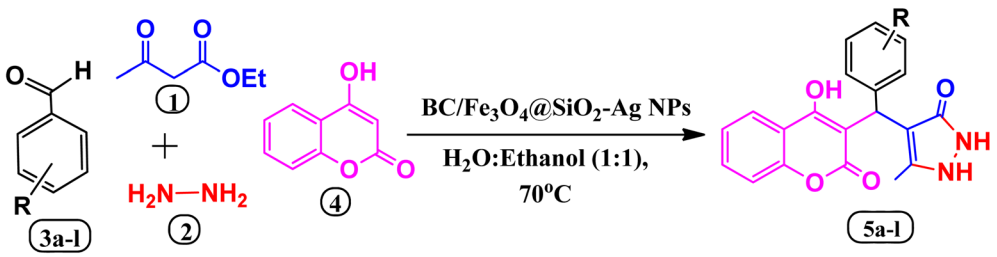

Entry	Biochar/Fe_3O_4@SiO_2–Ag NPs (mg)	Time (min)	Yield[b] %
1	None	120	0
2	0.5 mg	60	55
3	1 mg	20	75
4	2 mg	15	84
5	4 mg	15	89
6	**5 mg**	**12**	**97**
7	6 mg	15	95
8	7 mg	20	92
9	10 mg	20	79
10	Only biochar, 5 mg	50	45
11	Biochar/Fe_3O_4, 5 mg	30	75
12	Biochar/Fe_3O_4@SiO_2	30	87

[a] Condition; H_2O : EtOH (1 : 1) at 70 °C. [b] Isolated yield.

Table 3 Synthesis of benzylpyrazolyl coumarin derivatives (5a–l) using biochar/Fe_3O_4@SiO_2–Ag MNC

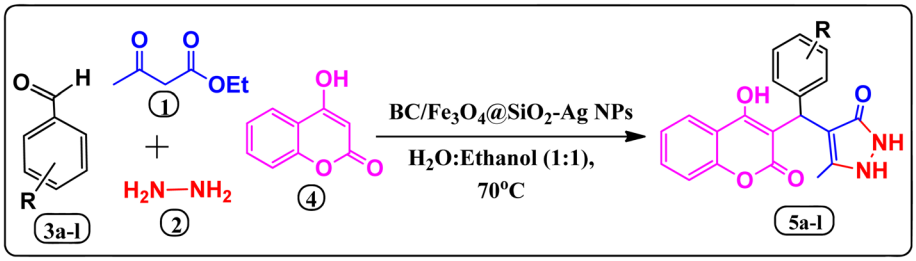

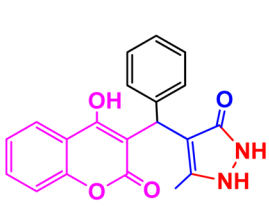

5a

12 min / 97%
M.P.: 231-233 [60,2]

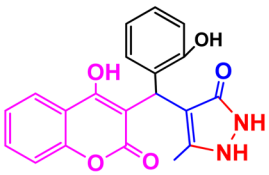

5b

13 min / 92%
M.P.: 220-222 [60]

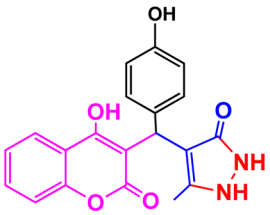

5c

16 min / 93%
M.P.: 224-226 [2]

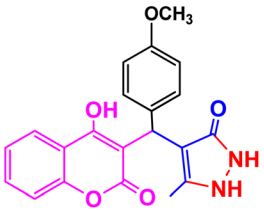

5d

18 min / 92%
M.P.: 201-203 [42]

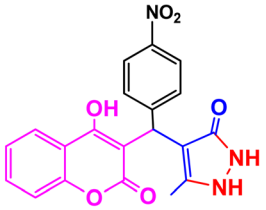

5e

13 min / 95%
M.P.: 209-211 [42]

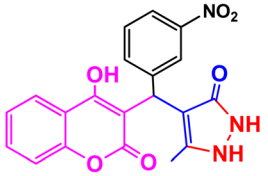

5f

14 min / 94%
M.P.: 206-208[42]

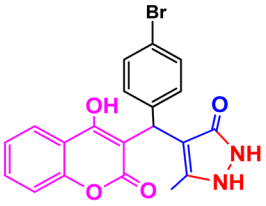

5g

17 min / 93%
M.P.: 231-233 [59,60]

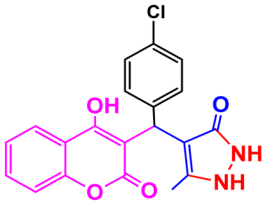

5h

15 min / 95%
M.P.: 215-217 [59,60]

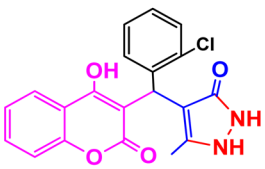

5i

16 min / 94%
M.P.: 221-222 [59,60]

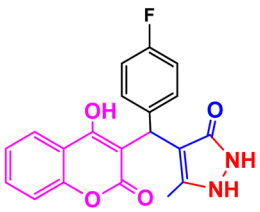

5j

18 min / 92%
M.P.: 237-238 [35,59,60]

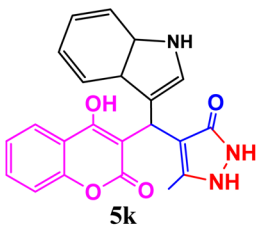

5k

17 min / 92%
M.P.: 236-238 [35,59,60]

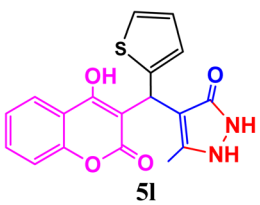

5l

16 min / 93%
M.P.: 221-223 [60]

(Table 1, entry 6–8) using EtOH : H_2O(1 : 1) as solvent but did not significantly promote the reaction. In addition, the ratio of the water and ethanol was varies with different temperature range (Table 1, entry 9–13) then EtOH : H_2O (1 : 1) was found to be the optimum solvent at 70 °C for these reactions (Table 1, entry 9).

Table 4 Comparative study with a reported method for the synthesis of benzylpyrazolyl coumarin derivatives

Entr y	Catalyst and solvent	Temp	Time (min)	Yield (%)	References
1	Taurine, H_2O	70 °C	20	92	59
2	$FeCl_3$–SiO_2, solvent free	110 °C	12	92	60
3	GL. AcOH, H_2O	Reflux	35	91	61
4	Fe_3O_4@SiO_2@PTS-DABA, EtOH : H_2O (1 : 1)	70 °C	30	91	62
5	CaO@walnut husk@ZnO, EtOH : H_2O (1 : 1)	70 °C	15	95	2
6	**Biochar/Fe_3O_4@SiO_2–Ag MNPs**	**70 °C**	**12**	**97**	**This work**

For further investigation, we than applied biochar, biochar/Fe_3O_4, and biochar/Fe_3O_4@SiO_2 as catalyst for the model reaction in EtOH : H_2O (1 : 1) for suitable time provided a 45%, 75%, and 87% amount of the desired product respectively (Table 2, entry 10–12). The quantity of the catalyst had a large effect on the formation of the desired product (Table 2). The catalyst was evaluated in various concentrations ranging from 1 to 10 mg in the following step as Table 2. The best outcomes, as seen in Table 2, came from utilizing 5 mg of the catalyst gives 97% amount of the desired product. Finally, the reaction was performed at temperatures between room temperature and 100 °C to determine the impact of temperature (Table 1, entry 1–13). At 70 °C, the model reaction produced the best results (Table 1, entry 9). The optimum result for the model reaction was achieved utilizing 5 mg of nanocatalyst at 70 °C in EtOH : H_2O (1 : 1) as a solvent to obtain the desired product in good to high yield. The outcomes show that biochar treated with Fe_3O_4, SiO_2, and Ag NPs have increased catalytic activity. The yield of benzylpyrazolyl coumarin analogs is lower when using biochar as a carrier for Fe_3O_4 NPs, as it is primarily used to prevent the aggregation of magnetic nanoparticles and provide a large specific surface area with surface functional groups (C=O, COOH, and OH), but does not exhibit significant catalytic activity (yield 45%). To improve catalytic activity and reusability, Fe_3O_4 NPs were introduced, allowing the catalyst to be recovered and reused with the aid of an external magnetic field. Additionally, Fe_3O_4 belongs to the spinel group with a standard formula of $A(B)_2O_4$, where A and B represent certain metal ions occupying specific locations in the crystal structure. Fe_3O_4's A and B metals are Fe^{2+} and Fe^{3+}, respectively, which causes the transfer of electrons in an organized path or vector between the different irons, generating a magnetic field from this electric vector. Furthermore, Fe^{2+} and Fe^{3+3+} have vacant d orbitals contributing to Fe_3O_4's Lewis acid characteristics (yield 75%). To prevent the aggregation of Fe_3O_4 nanoparticles, silica is employed as a protective covering shell for Fe_3O_4 NPs. The high concentration of Si–OH groups on the surface of silica allows for further modification using silicon reagents bearing organic bridges and suitable functional groups for subsequent modifications. In the presence of biochar/Fe_3O_4@SiO_2, the yield percentage increases as compared to biochar/Fe_3O_4 NPs (yield: 87%). Finally, Ag nanomaterials act as Lewis acids to activate the carbonyl groups of the aldehyde and ethylacetoacetate, enhancing the catalytic activity compared to other materials, with a maximum yield of 97%.

For Fe_3O_4 NPs, silica is also employed as a protective covering shell, and the silica shell can prevent the aggregation of Fe_3O_4 nanoparticles. Furthermore, the high concentration of Si–OH groups on the surface of silica allows for further modification, especially by silicon reagents bearing organic bridges and suitable functional groups for subsequent modifications. So in the presence of biochar/Fe_3O_4@SiO_2, the percentage of yield increases as compared to biochar/Fe_3O_4 NPs (yield: 87%). Finally, Ag nanomaterials also act as Lewis acids to activate the carbonyl groups of the aldehyde and ethylacetoacetate and improve the catalytic activity as compared to other materials, with a maximum yield of 97% obtained (Table 2). Numerous aromatic aldehydes with either electron-withdrawing or electron-donating properties were looked at to obtain the desired products after determining the best reaction conditions to study the scope and limitations of this approach (Table 3). It has been observed that all of the different substrates could be easily converted to the corresponding benzylpyrazolyl coumarins with good to excellent yields.

Additionally, the catalytic activity of biochar/Fe_3O_4@SiO_2–Ag nano-composite in the model reaction was compared with that of published studies (Table 4). According to the data in Table 4, the catalytic activity of biochar/Fe_3O_4@SiO_2–Ag MNPs is superior to CaO@walnut husk@ZnO, Fe_3O_4@SiO_2@PTS-DABA, GL. AcOH, and Taurine catalysts (entry 1–5) in terms of short reaction times, high yields, straightforward processes, and environmentally friendly conditions for the synthesis of benzylpyrazolyl coumarins. These advantages result from the high surface area and inherent porosity of Biochar/Fe_3O_4@-SiO_2–Ag MNPs.

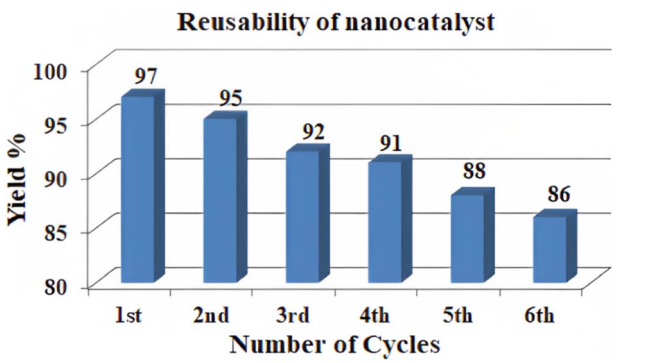

Fig. 14 The recyclability study of biochar/Fe_3O_4@SiO_2–Ag MNPs under optimal condition for model reaction (**5a**).

Recyclability and reusability of nanocatalyst

Under optimal conditions, the model reaction was used to investigate the recyclability of the biochar/Fe_3O_4@SiO_2–Ag catalyst. The catalyst was collected from the reaction mixture by using external magnet after the reaction was completed, washed with ethanol, dried under vacuum (60 °C), and evaluated for activity in five independent runs of the next reaction under the same reaction conditions. The plotted data (Fig. 14) show that during the period of the five runs, the catalytic activity of the biochar/Fe_3O_4@SiO_2–Ag MNPs has changed slightly. The FT-IR spectra were utilised to examine the structure of fresh and reused catalyst and can be shown in Fig. 6(b) and (c) that there were no changes after 5 runs.

Suggested reaction mechanism

In Scheme 2(A) and (B), it is proposed a plausible mechanism for the synthesis of benzylpyrazolyl coumarin derivatives with biochar/Fe_3O_4@SiO_2–Ag MNPs. The carbonyl groups of the aldehyde and ethylacetoacetate are activated during the process by catalyst, which functions as a Lewis acid. Intermediates (I) are produced by the nucleophilic attack of 4-hydroxy-coumarin on the activated carbonyl group of aldehyde and the subsequent removal of water. Moreover, the nucleophilic reaction between hydrazine and the activated carbonyl groups of ethyl acetoacetate produced the pyrazolone intermediate (II). After that, a Michael addition reaction between the intermediates (I) and (II) results in (III). Finally, the required product is then produced $^{by\ an}$ oxidation in the presence of biochar/Fe_3O_4@SiO_2–Ag magnetic nanocatalyst (Scheme 2A). Another alternative chemical pathway involves the synthesis of the intermediate (IV), which is then combined with 4-hydroxycoumarin to produce final product (Scheme 2B). These results revealed that intermediates (II) and (IV) were both very reactive towards the subsequent reaction with pyrazolone and 4-hydroxycoumarin respectively.

Results of anti-microbial activity

The antimicrobial activities of synthesized benzylpyrazolyl coumarins derivatives (**5a–l**) were tested against Gram-positive bacteria (*Staphylococcus aureus* and *Streptococcus pyogenes*), Gram-negative bacteria (*Escherichia coli* and *Pseudomonas aeruginosa*), and fungus (*Candida albicans, and Aspergillus niger*).

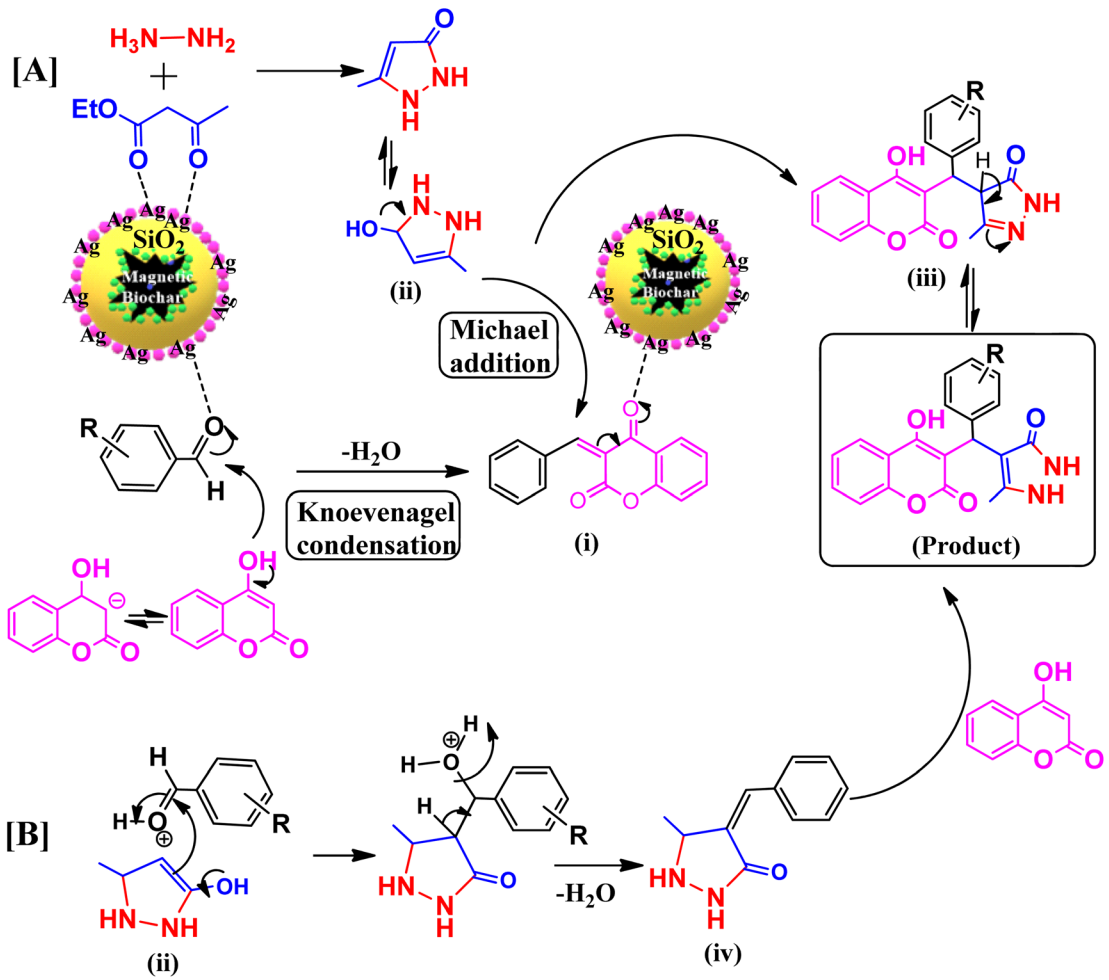

Scheme 2 (A) and (B) The plausible mechanism for the synthesis of benzylpyrazolyl coumarins in the presence of biochar/Fe_3O_4@SiO_2–Ag MNPs.

Table 5 Antibacterial activity of synthesized compound (**5a–5l**)

Antibacterial activity table				
Compound	*E. coli* [MTCC 443]	*P. aeruginosa* [MTCC 1688]	*S. aureus* [MTCC96]	*S. pyogenus* [MTCC 442]
Minimal inhibition concentration [μg ml^{-1}]				
5a	62.5	100	100	50
5b	31.25	50	125	100
5c	100	62.5	125	125
5d	62.5	125	100	125
5e	125	100	250	250
5f	100	250	100	125
5g	125	100	250	125
5h	100	125	100	50
5i	100	125	125	125
5j	125	125	250	125
5k	31.25	62.5	50	50
5l	62.5	100	125	100
Standard drugs [minimal bactericidal concentration] (μg ml^{-1})				
Ampicillin	100	100	250	100
Ciprofloxacin	25	25	50	50
Norfloxacin	10	10	10	10

To measure antibacterial activity, the broth dilution method was utilised, and DMSO was used as a diluent to achieve the ideal concentration of drugs for testing on common bacterial strains. Standard drugs such ampicillin, ciprofloxacin, norfloxacin, nystatin, and griseofulvin were used for antibacterial and antifungal studies. The lowest concentration that prevented the organism's growth was determined as the minimal inhibitory concentration (MIC) (Tables 5 and Table 6). According to the results, compound **5k** (MIC value 31.25 μg ml^{-1}, 62.5 μg ml^{-1}, 50 μg ml^{-1} and 50 μg ml^{-1} respectively) exhibited excellent antibacterial activity against *E. coli*, *P. aeruginosa*, *S. aureus*, and *S. pyogenes*. All compounds excluding **5e**, **5g**, and **5j** were shown very good antibacterial activity against *E. coli.* Compounds **5b**, **5c**, and **5k** (MIC value 50 μg ml^{-1} and 62.5 μg ml^{-1}) showed very good antibacterial activity as compared to ampicillin against *P. aeruginosa.* Compounds including **5f**, **5h**, **5k**, and **5l** had good antibacterial activity against *S. aureus*. All compounds (**5a–l**) exhibited good antifungal activity against *C. albicans* compared to standard drug griseofulvin.

Table 6 Antifungal activity of synthesized compounds (**5a–5l**)

Compound	*C. albicans* [MTCC 227]	*A. niger* [MTCC 282]
Antifungal activity table minimal fungicidal concentration [μg ml^{-1}]		
5a	250	250
5b	500	500
5c	250	250
5d	500	500
5e	500	1000
5f	250	500
5g	500	500
5h	500	250
5i	250	500
5j	500	1000
5k	125	250
5l	250	500
Standard drugs [inimal fungicidal concentration] (μg ml^{-1})		
Nystatin	100	100
Griseofulvin	500	100

Conclusion

We have developed a greener and more effective method of producing pharmacologically active benzylpyrazolyl coumarins derivatives (**5a–l**) with highest yields (91–98%) by a one-pot, four-component reaction of 4-hydroxycoumarin, ethyl acetoacetate, hydrazine hydrate and aromatic aldehydes in the presence of H_2O : EtOH (1 : 1) solvent at 70 °C. The reaction was catalysed by biochar/Fe_3O_4@SiO_2–Ag MNPs. The catalyst can be reused and recycled up to five times with good yield and no loss of catalytic activity. This method also makes it simple to separate the catalyst from the reaction mixture using an external magnet. This method's attractive qualities include excellent atom economy, a quick reaction time, good yields, and a greener reaction profile. Antimicrobial activity was tested on the resulting products (**5a–5l**). The studies show that the synthesised compounds exhibit significant antimicrobial activity against the fungus *Candida albicans*, the Gram-negative bacteria *E. coli* and *P. aeruginosa*, and the Gram-positive bacteria *S. aureus* and *S. phyogens*.

Conflicts of interest

The authors declare no conflict of interest, financial or otherwise.

Acknowledgements

Dharmendra gratefully acknowledge the council of scientific and industrial research (CSIR), New Delhi for award research fellowship (CSIR Award no.: 09/172(0093)/2019-EMR-I) for financial support. Thank you very much to the Department of chemistry and physics for providing us the NMR, FT-IR, TGA and XRD spectra facilities at MLSU (Mohanlal Sukhadia University). I admire the efforts of the PU facilities (SAIF and CIL Chandigarh) for providing timely services of HR-TEM and FE-SEM. I'd want to express my gratitude to IIT Roorkee for giving VSM facility. All the authors are highly thankful to the Ministry of Education and SPD-RUSA Rajasthan for financial support received under RUSA-2.0 Project.

References

1 P. Anastas and N. Eghbali, Green chemistry: principles and practice, *Chem. Soc. Rev.*, 2010, **39**(1), 301–312.
2 M. Hamzehniya, A. Mobinikhaledi, N. Ahadi and F. Sameri, Zn complexed on CaO coated with walnut husk extract as an efficient and reusable catalyst for the green synthesis of benzylpyrazolyl coumarin derivatives, *React. Kinet. Mech. Catal.*, 2022, **135**(2), 897–914.
3 J. Liu, J. Jiang, Y. Meng, A. Aihemaiti, Y. Xu, H. Xiang, Y. Gao and X. Chen, Preparation, environmental application and prospect of biochar-supported metal nanoparticles: a review, *J. Hazard. Mater.*, 2020, **388**, 122026.
4 D. Dharmendra, P. Chundawat, Y. Vyas and C. Ameta, Ultrasound-assisted efficient synthesis and antimicrobial evaluation of pyrazolopyranopyrimidine derivatives using starch functionalized magnetite nanoparticles as a green biocatalyst in water, *J. Chem. Sci.*, 2022, **134**(2), 1–22.
5 D. J. Roman and M. Yus, Asymmetric multicomponent reactions (AMCRs): the new frontier, *Angew. Chem., Int. Ed.*, 2005, **44**(11), 1602–1634.
6 T. Deligeorgiev, N. Gadjev, A. Vasilev, S. Kaloyanova, J. J. Vaquero and J. Alvarez-Builla, Green chemistry in organic synthesis, *Mini-Rev. Org. Chem.*, 2010, **7**(1), 44–53.
7 D. Akhil, D. Lakshmi, A. Kartik, D. V. N. Vo, J. Arun and K. P. Gopinath, Production, characterization, activation and environmental applications of engineered biochar: a review, *Environ. Chem. Lett.*, 2021, **19**(3), 2261–2297.
8 R. P. Lopes, T. Guimarães and D. Astruc, Magnetized biochar as a gold nanocatalyst support for p-nitrophenol reduction, *J. Braz. Chem. Soc.*, 2021, **32**, 1680–1686.
9 H. Lyu, Q. Zhang and B. Shen, Application of biochar and its composites in catalysis, *Chemosphere*, 2020, **240**, 124842.
10 Y. Y. Wang, L. L. Ling and H. Jiang, Selective hydrogenation of lignin to produce chemical commodities by using a biochar supported Ni–Mo_2 C catalyst obtained from biomass, *Green Chem.*, 2016, **18**(14), 4032–4041.
11 J. L. Vidal, V. P. Andrea, S. L. MacQuarrie and F. M. Kerton, Oxidized biochar as a simple, renewable catalyst for the production of cyclic carbonates from carbon dioxide and epoxides, *ChemCatChem*, 2019, **11**(16), 4089–4095.
12 S. Z. Zhang, Z. S. Cui, M. Zhang and Z. H. Zhang, Biochar based functional materials as heterogeneous catalysts for organic reactions, *Curr. Opin. Green Sustainable Chem.*, 2022, 100713.
13 L. N. Dong, Y. M. Wang, W. L. Zhang, L. P. Mo and Z. H. Zhang, Nickel supported on magnetic biochar as a highly efficient and recyclable heterogeneous catalyst for the one-pot synthesis of spirooxindole-dihydropyridines, *Appl. Organomet. Chem.*, 2022, **36**(5), e6667.
14 P. Moradi and M. Hajjami, Stabilization of ruthenium on biochar-nickel magnetic nanoparticles as a heterogeneous, practical, selective, and reusable nanocatalyst for the Suzuki C–C coupling reaction in water, *RSC Adv.*, 2022, **12**(21), 13523–13534.
15 L. N. Dong, S. Z. Zhang, W. L. Zhang, Y. Dong, L. P. Mo and Z. H. Zhang, Synthesis, characterization and application of magnetic biochar sulfonic acid as a highly efficient recyclable catalyst for preparation of spiro-pyrazolo [3, 4-b] pyridines, *Res. Chem. Intermed.*, 2022, **48**(3), 1249–1272.
16 D. Dharmendra, P. Chundawat, Y. Vyas, P. Chaubisa, M. Kumawat and C. Ameta, Eco-friendly design of TiO_2 nanoparticles supported on Fe_3O_4 coated carbon-based biochar substrate for the synthesis of pyrano-[2, 3-c]-pyrazole derivatives, *Sustainable Chem. Pharm.*, 2022, **28**, 100732.
17 R. Ghosh, L. Pradhan, Y. P. Devi, S. S. Meena, R. Tewari, A. Kumar, S. Sharma, N. S. Gajbhiye, R. K. Vatsa, B. N. Pandey and R. S. Ningthoujam, Induction heating studies of Fe3O4 magnetic nanoparticles capped with oleic acid and polyethylene glycol for hyperthermia, *J. Mater. Chem.*, 2011, **21**(35), 13388–13398.
18 Z. Alirezvani, M. G. Dekamin and E. Valiey, Cu (II) and magnetite nanoparticles decorated melamine-functionalized chitosan: a synergistic multifunctional catalyst for sustainable cascade oxidation of benzyl alcohols/Knoevenagel condensation, *Sci. Rep.*, 2019, **9**(1), 1–12.
19 F. Davoodi, M. G. Dekamin and Z. Alirezvani, A practical and highly efficient synthesis of densely functionalized nicotinonitrile derivatives catalyzed by zinc oxide-decorated superparamagnetic silica attached to graphene oxide nanocomposite, *Appl. Organomet. Chem.*, 2019, **33**(4), e4735.
20 M. Ishani, M. G. Dekamin and Z. Alirezvani, Superparamagnetic silica core–shell hybrid attached to graphene oxide as a promising recoverable catalyst for expeditious synthesis of TMS-protected cyanohydrins, *J. Colloid Interface Sci.*, 2018, **521**, 232–241.
21 V. Polshettiwar, R. Luque, A. Fihri, H. Zhu, M. Bouhrara and J. M. Basset, Magnetically recoverable nanocatalysts, *Chem. Rev.*, 2011, **111**(5), 3036–3075.
22 S. Shylesh, V. Schünemann and W. R. Thiel, Magnetically separable nanocatalysts: bridges between homogeneous and heterogeneous catalysis, *Angew. Chem., Int. Ed.*, 2010, **49**(20), 3428–3459.
23 R. Mohammadi, S. Esmati, M. Gholamhosseini-Nazari and R. Teimuri-Mofrad, Synthesis and characterization of

a novel Fe_3O_4@SiO_2–BenzIm-Fc [Cl]/BiOCl nano-composite and its efficient catalytic activity in the ultrasound-assisted synthesis of diverse chromene analogs, *New J. Chem.*, 2019, **43**(1), 135–145.

24 S. Karami, M. G. Dekamin, E. Valiey and P. Shakib, DABA MNPs: A new and efficient magnetic bifunctional nanocatalyst for the green synthesis of biologically active pyrano [2, 3-c] pyrazole and benzylpyrazolyl coumarin derivatives, *New J. Chem.*, 2020, **44**(33), 13952–13961.

25 Y. H. Deng, C. C. Wang, J. H. Hu, W. L. Yang and S. K. Fu, Investigation of formation of silica-coated magnetite nanoparticles via sol–gel approach, *Colloids Surf., A*, 2005, **262**(1–3), 87–93.

26 A. L. Morel, S. I. Nikitenko, K. Gionnet, A. Wattiaux, J. Lai-Kee-Him, C. Labrugere, B. Chevalier, G. Deleris, C. Petibois, A. Brisson and M. Simonoff, Sonochemical approach to the synthesis of Fe_3O_4@SiO_2 core–shell nanoparticles with tunable properties, *ACS Nano*, 2008, **2**(5), 847–856.

27 H. Hu, Z. Wang, L. Pan, S. Zhao and S. Zhu, Ag-coated Fe_3O_4@SiO_2 three-ply composite microspheres: synthesis, characterization, and application in detecting melamine with their surface-enhanced Raman scattering, *J. Phys. Chem. C*, 2010, **114**(17), 7738–7742.

28 H. L. Qin, Z. W. Zhang, L. Ravindar and K. P. Rakesh, Antibacterial activities with the structure-activity relationship of coumarin derivatives, *Eur. J. Med. Chem.*, 2020, **207**, 112832.

29 B. H. Lee, M. F. Clothier, F. E. Dutton, G. A. Conder and S. S. Johnson, Anthelmintic β-hydroxyketoamides (BKAS), *Bioorg. Med. Chem. Lett.*, 1998, **8**, 3317–3320.

30 P. P. Ghosh, G. Pal, S. Paul and A. R. Das, Design and synthesis of benzylpyrazolyl coumarin derivatives via a four-component reaction in water: investigation of the weak interactions accumulating in the crystal structure of a signified compound, *Green Chem.*, 2012, **14**(10), 2691–2698.

31 S. Hesse and G. Kirsch, A rapid access to coumarin derivatives (using Vilsmeier–Haack and Suzuki cross-coupling reactions), *Tetrahedron Lett.*, 2002, **43**, 1213–1215.

32 G. Melagraki, A. Afantitis, O. Igglessi-Markopoulou, A. Detsi, M. Koufaki, C. Kontogiorgis and D. J. Hadjipavlou-Litina, Synthesis and evaluation of the antioxidant and anti-inflammatory activity of novel coumarin-3-aminoamides and their alpha-lipoic acid adducts, *Eur. J. med. Chem.*, 2009, **44**(7), 3020–3026.

33 N. A. A. Latif, R. Z. Batran, M. A. Khedr and M. M. Abdalla, 3-Substituted-4-hydroxycoumarin as a new scaffold with potent CDK inhibition and promising anticancer effect: Synthesis, molecular modeling and QSAR studies, *Bioorg. Chem.*, 2016, **67**, 116–129.

34 M. A. Musa, J. S. Cooperwood and M. O. F. Khan, A review of coumarin derivatives in pharmacotherapy of breast cancer, *Curr. Med. Chem.*, 2008, **15**, 2664–2679.

35 A. P. Katariya, S. U. Deshmukh, S. U. Tekale, M. V. Katariya and R. P. Pawar, Amberlite IR-120 catalyzed green and efficient one-pot synthesis of benzylpyrazolyl coumarin in aqueous medium, *Lett. Appl. NanoBioScience*, 2021, **10**, 2525–2534.

36 D. Srikrishna, S. Tasqeeruddin and P. K. Dubey, Synthesis of 3 -substituted coumarins: an efficient green approach using L-proline as catalyst in triethanolamine medium, *Lett. Org. Chem.*, 2014, **11**, 556–563.

37 R. Y. Guo, Z. M. An, L. P. Mo, S. T. Yang, H. X. Liu, S. X. Wang and Z. H. Zhang, Meglumine promoted one-pot, four-component synthesis of pyranopyrazole derivatives, *Tetrahedron*, 2013, **69**(47), 9931–9938.

38 N. Kerru, L. Gummidi, S. Maddila, K. K. Gangu and S. B. Jonnalagadda, A review on recent advances in nitrogen-containing molecules and their biological applications, *Molecules*, 2020, **25**(8), 1909.

39 G. Akerlof, Dielectric constants of some organic solvent-water mixtures at various temperatures, *J. Am. Chem. Soc.*, 1932, **54**(11), 4125–4139.

40 S. M. Mejía, E. Flórez and F. Mondragón, An orbital and electron density analysis of weak interactions in ethanol-water, methanol-water, ethanol and methanol small clusters, *J. Chem. Phys.*, 2012, **136**(14), 144306.

41 R. A. Sheldon, The greening of solvents: towards sustainable organic synthesis, *Curr. Opin. Green Sustainable Chem.*, 2019, **18**, 13–19.

42 M. M. Heravi, R. Malakooti, K. Kafshdarzadeh, Z. Amiri, V. Zadsirjan and H. Atashin, Supported palladium oxide nanoparticles in Al-SBA-15 as an efficient and reusable catalyst for the synthesis of pyranopyrazole and benzylpyrazolyl coumarin derivatives via multicomponent reactions, *Res. Chem. Intermed.*, 2022, **48**(1), 203–234.

43 Y. Tian, M. Wu, X. Lin, P. Huang and Y. Huang, Synthesis of magnetic wheat straw for arsenic adsorption, *J. Hazard. Mater.*, 2011, **193**, 10–16.

44 S. A. Baig, Z. Lou, M. T. Hayat, R. Fu, Y. Liu and X. Xu, Characterization of magnetic biochar amended with silicon dioxide prepared at high temperature calcination, *Mater. Sci.-Pol.*, 2016, **34**(3), 597–604.

45 C. Duran and D. Ozdes, Application of Magnetic Fe_3O_4 Alnus glutinosa Sawdust Biochar/SiO_2/CTAB as a New Sorbent for Magnetic Solid Phase Extraction of Heavy Metals from Fruit and Waters Samples, *Int. J. Environ. Anal. Chem.*, 2021, 1–19.

46 Y. Chi, Q. Yuan, Y. Li, J. Tu, L. Zhao, N. Li and X. Li, Synthesis of Fe_3O_4@SiO_2–Ag magnetic nanocomposite based on small-sized and highly dispersed silver nanoparticles for catalytic reduction of 4-nitrophenol, *J. Colloid Interface Sci.*, 2012, **383**(1), 96–102.

47 P. Mukherjee, M. Roy, B. P. Mandal, G. K. Dey, P. K. Mukherjee, J. Ghatak, A. K. Tyagi and S. P. Kale, Green synthesis of highly stabilized nanocrystalline silver particles by a non-pathogenic and agriculturally important fungus T. asperellum, *Nanotechnology*, 2008, **19**(7), 075103.

48 J. Zou, T. Xu, B. Hou, D. Wu and Y. Sun, Controlled growth of silver nanoparticles in a hydrothermal process, *China Particuol.*, 2007, **5**, 206–212.

49 B. Kumar, K. Smita, L. Cumbal, A. Debut and R. N. Pathak, Sonochemical synthesis of silver nanoparticles using starch: a comparison, *Bioinorg. Chem. Appl.*, 2014, 784268.
50 B. Kumar, K. Smita, L. Cumbal and A. Debut, Green synthesis of silver nanoparticles using Andean blackberry fruit extract, *Saudi J. Biol. Sci.*, 2017, **24**(1), 45–50.
51 Y. Chen, H. Ding and S. Sun, Preparation and characterization of ZnO nanoparticles supported on amorphous SiO_2, *Nanomaterials*, 2017, **7**(8), 217–229.
52 M. Abou Abou Rida and F. Harb, Synthesis and characterization of amorphous silica nanoparticles from aqueous silicates using cationic surfactants, *J. Met. Mater. Miner.*, 2014, **24**(1), 37–42.
53 X. Pan, Z. Gu, W. Chen and Q. Li, Preparation of biochar and biochar composites and their application in a Fenton-like process for wastewater decontamination: a review, *Sci. Total Environ.*, 2021, **754**, 142104.
54 C. Ma, C. Li, N. He, F. Wang, N. Ma, L. Zhang, Z. Lu, Z. Ali, Z. Xi, X. Li and G. Liang, Preparation and characterization of monodisperse core–shell Fe_3O_4@SiO_2 microspheres and its application for magnetic separation of nucleic acids from E. coli BL21, *J. Biomed. Nanotechnol.*, 2012, **8**(6), 1000–1005.
55 M. Gao, W. Li, J. Dong, Z. Zhang and B. Yang, Synthesis and characterization of superparamagnetic Fe_3O_4@SiO_2 core–shell composite nanoparticles, *World J. Condens. Matter Phys.*, 2011, **1**(2), 49–54.
56 A. Kohzadian and H. Filian, Production and characterization of Fe_3O_4@SiO_2@TMEDA-Pd as a very effectual interphase catalyst for the rapid preparation of di-aryl sulfides and pyrido-dipyrimidines, *Silicon*, 2023, 1–16.
57 I. D. Inaloo, S. Majnooni, H. Eslahi and M. Esmaeilpour, Nickel(II) Nanoparticles Immobilized on EDTA-Modified Fe_3O_4@SiO_2 Nanospheres as Efficient and Recyclable Catalysts for Ligand-Free Suzuki–Miyaura Coupling of Aryl Carbamates and Sulfamates, *ACS Omega*, 2020, **5**(13), 7406–7417.
58 H. Rajabi-Moghaddam, M. R. Naimi-Jamal and M. Tajbakhsh, Fabrication of copper (II)-coated magnetic core-shell nanoparticles Fe_3O_4@SiO_2-2-aminobenzohydrazide and investigation of its catalytic application in the synthesis of 1, 2, 3-triazole compounds, *Sci. Rep.*, 2021, **11**(1), 1–14.
59 A. V. Chate, B. A. Shaikh, G. M. Bondle and S. M. Sangle, Efficient atom-economic one-pot multicomponent synthesis of benzylpyrazolyl coumarins and novel pyrano [2, 3-c] pyrazoles catalysed by 2-aminoethanesulfonic acid (taurine) as a bio-organic catalyst, *Synth. Commun.*, 2019, **49**, 2244–2257.
60 Z. Piruzmand, J. Safaei-Ghomi and M. Ghasemzadeh, A facile solvent-free route for the one-pot multicomponent synthesis of benzylpyrazolyl coumarins catalyzed by $FeCl_3$-SiO_2 nanoparticles, *Med. Chem.*, 2016, **9**, 619.
61 P. P. Ghosh, G. Pal, S. Paul and A. R. Das, Design and synthesis of benzylpyrazolyl coumarin derivatives via a four-component reaction in water: investigation of the weak interactions accumulating in the crystal structure of a signified compound, *Green Chem.*, 2012, **14**, 2691–2698.
62 S. Karami, M. G. Dekamin, E. Valiey and P. Shakib, DABA MNPs: a new and efficient magnetic bifunctional nanocatalyst for the green synthesis of biologically active pyrano [2, 3-c] pyrazole and benzylpyrazolyl coumarin derivatives, *New J. Chem.*, 2020, **44**, 13952–13961.